JGR Oceans

RESEARCH ARTICLE
10.1029/2025JC023089

Blue Carbon Ecosystems Modulate the Air-Sea CO_2 Exchange and Coastal Acidification in Tropical Estuaries

Jianzhong Su[1,2], Shimin Xiao[2], Cong Tan[2], Zhixiong Huang[2], Min Nina Xu[1,2], Ehui Tan[1,2], Liguo Guo[3], Guizhi Wang[3], Wei-Jun Cai[4], and Shuh-Ji Kao[2]

[1]School of Marine Science and Engineering, Hainan University, Haikou, China, [2]State Key Laboratory of Marine Resources Utilization in South China Sea, Hainan University, Haikou, China, [3]State Key Laboratory of Marine Environmental Science, Xiamen University, Xiamen, China, [4]School of Marine Science and Policy, University of Delaware, Newark, DE, USA

Abstract The diverse and productive blue carbon ecosystems (mangrove, seagrass, salt marsh, and macroalgae) provide many ecosystem services and play an important role in climate change mitigation and adaptation. However, less is known about how different biogeochemical processes within blue carbon ecosystems can influence seawater carbonate dynamics especially on the partial pressure of carbon dioxide (pCO_2) and pH. Through underway pCO_2 measurements and discrete water samples, we examined the spatial and temporal distributions of the carbonate system in two tropical mangrove estuaries and one benthic-macroalgae-vegetated lagoon. In early summer, the mangrove estuaries behaved as weak CO_2 sources of 2.0–4.0 mmol m^{-2} d^{-1}, whereas the tropical lagoon became a CO_2 sink of −6.4 mmol m^{-2} d^{-1}. The chemical stoichiometry, stable carbon isotope, and other geochemical tracers reveal that carbonate dissolution and sulfate reduction followed by aerobic respiration are dominant controls on carbonate dynamics in mangrove estuaries. Without alkalinity enhancement driven by carbonate dissolution and sulfate reduction mainly from mangrove sediments, CO_2 emission would be 23 times larger than current observation, and pH would decrease by 0.39 units on an estuary-wide scale. However, in macroalgae-inhabited lagoon primary production followed by carbonate formation could draw pCO_2 down to 70 μatm and raise pH to 8.8, which are significantly distinct from the normal estuarine water. This study demonstrates that lateral export of alkalinity from mangrove sediments and the in situ metabolism of macroalgae can significantly influence the estuarine air-sea CO_2 flux and acidification status, and emphasizes the importance of protecting and restoring the blue carbon ecosystems.

Plain Language Summary Blue carbon ecosystems provide vital services and help mitigate climate change. However, the effect of their internal biogeochemical processes on the coastal carbonate system is poorly understood. Our study shows that in early summer, waters in two tropical mangrove estuaries released CO_2 into the air, whereas water in the macroalgae-vegetated lagoon absorbed CO_2. In mangrove estuaries, carbonate dissolution and sulfate reduction (followed by aerobic respiration) primarily control the carbonate dynamics. If there is no alkalinity enhancement driven by these mangrove sediment processes, CO_2 emission would be 23 times higher and the estuary-wide pH would drop by 0.39 units. In contrast, benthic macroalgae in the lagoon took up CO_2 and raised pH through photosynthesis and carbonate formation. This demonstrates that alkalinity export from mangrove sediments and the in situ metabolism of macroalgae significantly influence the estuarine air-sea CO_2 exchange and acidification. Protecting and restoring these blue carbon ecosystems are therefore essential.

Key Points:

- Continuous underway measurements reveal that tidal movement significantly affects the spatial distributions of water properties
- Strong photosynthesis of benthic macroalgae turns the air-sea CO_2 status from a source into a sink in a eutrophic tropical lagoon
- Lateral export of alkalinity from mangrove sediments decreases the partial pressure of CO_2 and increases pH in the adjacent coastal sea

Supporting Information:

Supporting Information may be found in the online version of this article.

Correspondence to:

J. Su,
jzsu@hainanu.edu.cn

Citation:

Su, J., Xiao, S., Tan, C., Huang, Z., Xu, M. N., Tan, E., et al. (2025). Blue carbon ecosystems modulate the air-sea CO_2 exchange and coastal acidification in tropical estuaries. *Journal of Geophysical Research: Oceans*, *130*, e2025JC023089. https://doi.org/10.1029/2025JC023089

Received 1 JUL 2025
Accepted 30 AUG 2025

Author Contributions:

Conceptualization: Jianzhong Su
Data curation: Jianzhong Su, Shimin Xiao, Cong Tan, Zhixiong Huang, Liguo Guo
Funding acquisition: Jianzhong Su, Min Nina Xu, Ehui Tan, Shuh-Ji Kao
Investigation: Jianzhong Su, Shimin Xiao, Cong Tan, Zhixiong Huang
Writing – original draft: Jianzhong Su
Writing – review & editing: Jianzhong Su, Min Nina Xu, Ehui Tan, Guizhi Wang, Wei-Jun Cai, Shuh-Ji Kao

1. Introduction

Estuaries represent a biogeochemical active zone that transforms a significant amount of terrestrial material into the coastal ocean. Processing of the organic and inorganic carbon usually leads to a strongly heterotrophic water column and a high carbon dioxide (CO_2) emission toward the atmosphere. Although estuaries only account for 0.3% of the global ocean surface area, the estuarine CO_2 emissions were estimated as 0.1–0.34 Pg C yr^{-1} approximating the CO_2 uptake by continental shelves (Cai, 2011; C. T. A. Chen et al., 2013; Laruelle et al., 2013). However, such estimations have large uncertainties as past studies focused more on smaller river-dominant estuaries with high pCO_2 values (C. T. A. Chen et al., 2013). Large estuaries such as the Chesapeake Bay (B. Chen et al., 2020), the Delaware Bay (Joesoef et al., 2015), and larger lagoons (Koné et al., 2009) appear to behave as either a weak CO_2 source or even a CO_2 sink.

In addition, unlike the traditional ocean acidification induced by oceanic uptake of anthropogenic CO_2, the causes for coastal/estuarine acidification are more complex. The physical mixing between weakly buffered river water and well buffered seawater will form a minimum buffering zone that is extra sensitive to acid additions regardless of the acid source (Cai et al., 2021; X. Hu & Cai, 2013). Moreover, microbial respiration of excessive organic matter from eutrophication-induced primary production or nearby wetlands will enhance the acidification in coastal waters (Cai et al., 2011) seriously threatening the health of calcifying organisms and their habitats. Given the importance of estuarine CO_2 emissions and coastal acidification in the global carbon budget and climate change, a thorough understanding of carbon cycling in estuaries and the related controlling mechanisms remains a major challenge, in particular for the tropics, where about 60% of freshwater discharge and riverine total organic carbon export occur (Borges, 2005).

A wide range of tropical estuaries are accompanied by blue carbon ecosystems such as mangrove and seagrass beds, which are highly productive with high carbon sequestration rates disproportionate to their areas (Alongi, 2020). The metabolic activities and related biogeochemistry of these ecosystems can inevitably affect the carbon flow of the coastal zone. The larger lateral exports of total alkalinity (TA) than dissolved inorganic carbon (DIC) from mangrove sediments could promote CO_2 outgassing within the tidal creeks and create a measurable localized increase in adjacent coastal ocean pH, which has been previously documented by Sippo et al. (2016) in their study of Australian mangroves. The strong photosynthesis by seagrass meadows could largely draw down partial pressure of CO_2 (pCO_2), and raise pH in the overlying water over days or even months (Chou et al., 2021). Meanwhile, the calcium carbonate ($CaCO_3$) mineral produced under a high pH environment can either dissolve in the underlying seagrass sediment or be transported to hypoxic/anoxic bottom water for dissolution, increasing the capacity to absorb atmospheric CO_2 and alleviate pH reduction (J. Su, Cai, Brodeur, Chen, et al., 2020).

For blue carbon ecosystems, previous research has focused on quantifying the carbon stocks and burial rates in sediments or biomass accumulation (Alongi, 2014). In recent years, many efforts have been made to measure the CO_2 flux at the air-sea interface (Akhand et al., 2021; Call et al., 2015, 2019; Rosentreter et al., 2018), constrain the lateral export fluxes of different carbon components to coastal waters (X. Chen et al., 2018, 2021; Ray et al., 2020; Reithmaier et al., 2020; Santos et al., 2021), and differentiate the dominant metabolic processes for the outwelled materials (Reithmaier et al., 2023; Rosentreter & Eyre, 2025; Sippo et al., 2016). However, very few studies have quantitatively linked the specific biogeochemical processes within blue carbon ecosystems to the dynamics of carbonate parameters in the adjacent coastal waters especially pCO_2 and pH (Cotovicz et al., 2020; Volta et al., 2020). These links are essential to understand in the context of global climate change and declines of blue carbon ecosystems driven by anthropogenic activities (Fluet-Chouinard et al., 2023).

To understand how the diverse blue carbon ecosystems influence CO_2 emission and ocean acidification in adjacent coastal waters, we performed field surveys on the carbonate system in three tropical estuaries partially inhabited by mangroves and benthic macroalgae. Continuous underway pCO_2 measurements were conducted to quantify the CO_2 flux at the air-sea interface. Water column carbonate chemistry, two-endmember mixing model, and other geochemical tracers were applied to differentiate the dominant controls on the carbonate system. Based on the case study of a mangrove estuary (i.e., Qinglan Harbor), we performed a simplified simulation to quantify how different biogeochemical processes affect pCO_2 and pH. Our analysis supports that the blue carbon ecosystems can significantly modulate estuarine CO_2 emission and acidification, providing another valid rationale for their protection and restoration.

2. Materials and Methods

2.1. Site Descriptions

Located in southern China, Hainan Island is subject to a tropical monsoon climate, and about 80% of the precipitation occurs in the wet season (May–October). The three tropical estuaries lie on the northeastern and eastern shores of Hainan Island (Figure 1) with lengths of 12–17 km and surface areas of 23–43 km^2. The estuarine topography is shallow with mean water depths of 1–4 m except for the narrow deep tidal channels with depths <10 m. The estuaries receive low freshwater discharge with an annual mean of 20–30 $m^3\ s^{-1}$ from nearby small rivers and are characterized by the irregular semidiurnal tide with a tidal range of ∼1 m. On the broad intertidal zones, the mangrove coverage areas reach 16.6 km^2 in Dongzhai Harbor (20.00°N, 110.57°E) and ∼7.5 km^2 in Qinglan Harbor (19.60°N, 110.82°E) estimated from satellite images (Li et al., 2020). However, in the warm season, macroalgae can thrive at the bottom water of the southern Xiaohai Lagoon (18.84°N, 110.48°E)

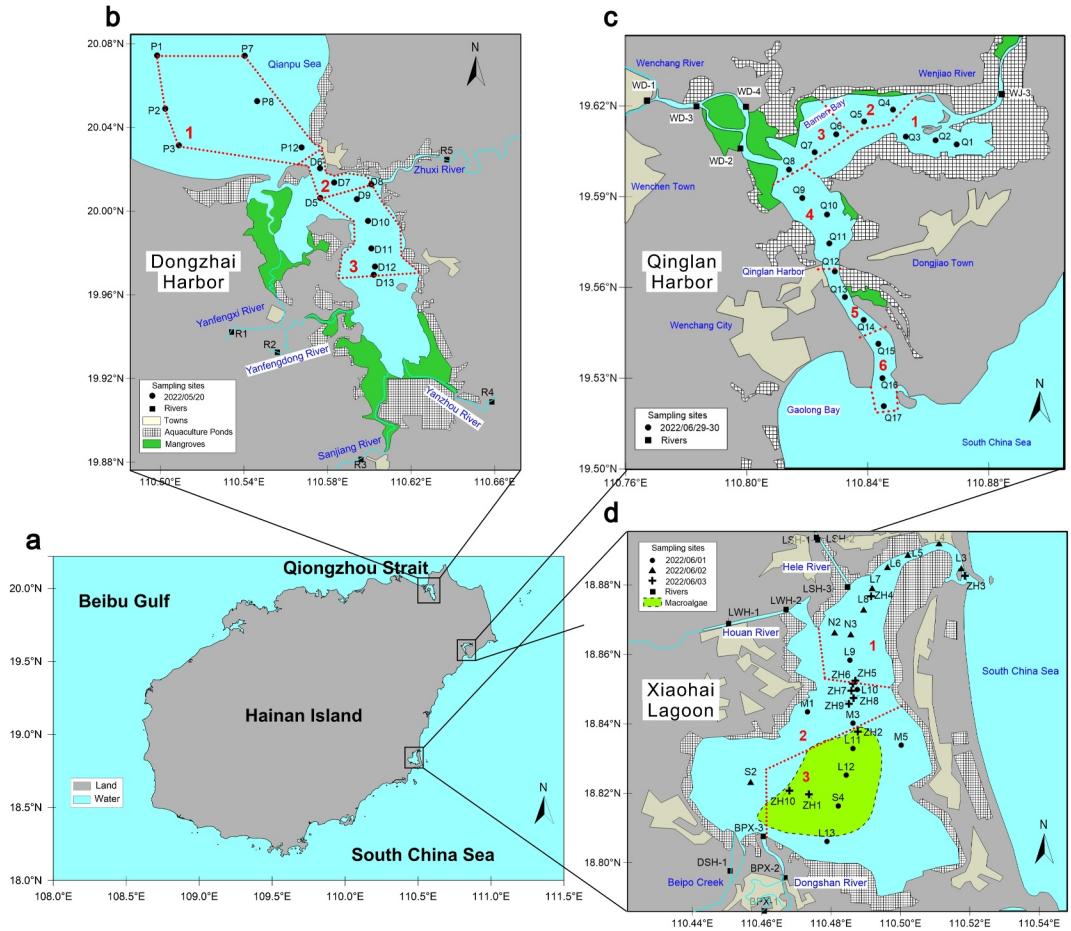

Figure 1. Sampling locations in three tropical estuaries in Hainan Island (a), China. The mangrove forests in Dongzhai Harbor (b) and Qinglan Harbor (c) are shaded in green colors, whereas the coverage of benthic macroalgae in Xiaohai Lagoon (d) is shaded in light green. According to the biogeochemical characteristics, the underway data are separated by the dotted lines into several domains, which are labeled by red numbers.

evidenced by low surface water pCO_2 (<200 μatm). All the estuaries are surrounded by many towns with large populations, thus suffering from intensified anthropogenic perturbations, such as agricultural drainage, domestic sewage, deforestation, and aquaculture waste (Liang et al., 2022; X. Liu & Ge, 2012; B. Liu et al., 2024). Billions of funds have been used by the government to remove the breeding ponds and mudflat aquaculture to restore the blue carbon ecosystems since 2019. More detailed site descriptions can be found in Text S1 in Supporting Information S1.

2.2. Underway pCO_2 Measurements

Cruises were conducted on 10-m-long boats in Dongzhai Harbor during flood tide on 20 May, in Qinglan Harbor during ebb tide on 29 June, and in Xiaohai Lagoon near slack high tide on 3 June 2022 (Figure S1 in Supporting Information S1). At each sampling campaign, water (~0.5 m below surface) was pumped continuously to the deck through a submersible pump and was distributed into three ways for an underway pCO_2 system (AS-P2, Apollo SciTech) at a flow rate of ~2.2 L min^{-1}, a multi-parameter CTD (Ocean Seven 310, IDRONAUT), and a drainage outlet. The differences in surface water temperature and salinity between the thermosalinograph inside the pCO_2 system (SBE45, Sea-Bird Scientific) and CTD are minor (Figure S2 in Supporting Information S1). The CO_2 mole fraction in dry air was detected by the nondispersive infrared (NDIR) spectrometer (LI-7000, LI-COR) approximately every 1.5 min. The NDIR detector was calibrated right before and after the cruise against three or four CO_2 gas standards (200, 400, 601, and 800 ppm), which are certified by the National Institute of Metrology, China. Atmospheric pCO_2 was also determined every 2.5 hr by the same pCO_2 system. The underway pCO_2

measurement has a precision of 0.1 µatm and an overall accuracy within 2 µatm. The dissolved oxygen (DO) optical sensor of CTD has a precision better than 0.025 mg L^{-1} and an initial accuracy of 0.1 mg L^{-1}. The precision and accuracy for pH sensor of CTD are 0.0001 and 0.01 units. Note that pH was also calculated from measured DIC and TA from discrete water samples on the National Institute of Standards and Technology scale via CO2SYS program (Xu et al., 2017). Calibrations of both sensors were carried out as described in the operator's manual before the cruises.

2.3. Discrete Sample Collection and Analysis

All discrete samples were taken above 5 m depth, and 88% of all were collected at the surface layer (<1 m) using a 5 L transparent acrylic water sampler. The practical salinity was measured by a salinometer (HI98192, HANNA instruments) with a precision of 0.01. The DIC and TA samples were collected in one 250 mL borosilicate glass bottle and preserved with 50 µL saturated $HgCl_2$ solution. These samples were first measured by a NDIR analyzer (AS-C3, Apollo SciTech) for DIC concentration and then were analyzed by Gran titration in an open-cell setting (AS-ALK2, Apollo SciTech) for TA concentration (Huang et al., 2012). The precision for triplicated DIC and duplicated TA analysis was ±0.1%. Both DIC and TA measurements were calibrated against certified reference materials from Andrew Dickson of the University of California at San Diego. We measured δ^{13}C-DIC samples by coupling a pretreatment device (AS-D1, Apollo SciTech) and a cavity ring-down spectrometer detector (G2131-i, Picarro) (J. Su et al., 2019). Each sample has two to three repeat runs with a precision better than 0.1‰. Three $NaHCO_3$ solutions with known δ^{13}C-DIC values (−12.20, −8.62, 0.84‰) were used as homemade standards to perform calibrations. We measured Ca^{2+} samples using an auto-titration technique modified from Kanamori and Ikegami (1980) with a precision better than 0.1%.

2.4. Estimation of the Air-Sea CO_2 Flux

CO_2 fluxes in units of mmol m^{-2} d^{-1} were estimated based on the following equation:

$$F = k \times K_0 \times \left(pCO_2^{water} - pCO_2^{air}\right) \quad (1)$$

where k is the gas transfer velocity of CO_2 in cm h^{-1}, K_0 is the solubility of CO_2 in mol kg^{-1} atm^{-1} (Weiss, 1974), and pCO_2^{water} and pCO_2^{air} are in situ pCO_2 in surface water and cruise mean atmospheric pCO_2 in µatm. A positive value indicates net flux from water to air. The k in coastal estuaries is affected by many factors, such as wind speed, current velocity, and water depth and seems site-specific (Borges et al., 2004; Ho et al., 2016; Rosentreter et al., 2017). Unfortunately, we did not collect the current velocity data. Instead, three different empirically derived k models based on wind speed were used to provide a possible range in CO_2 flux. The k_{600} parameterization of Raymond and Cole (2001) (RC01) was derived from many studies in rivers and estuaries using floating chamber and gas tracers.

$$k_{600}(\mathrm{R01}) = 1.91e^{0.35U_{10}} \quad (2)$$

The U_{10} is the wind speed at 10 m above the sea surface. The wind-speed k_{600} relationship proposed by Borges et al. (2004) (B04) was derived from a large set of flux measurements made by floating chamber in a macrotidal estuary.

$$k_{600}(\mathrm{B04}) = 1.0 + 2.58U_{10} \quad (3)$$

The k_{600} model of Jiang et al. (2008) (J08) was produced by regressing the literature data in coastal environments.

$$k_{600}(\mathrm{J08}) = 3.990 - 0.436U_{10} + 0.314U_{10}^2 \quad (4)$$

In addition, we applied another two k parameterizations of Wanninkhof (1992) (W92) and Wanninkhof (2014) (W14) derived for oceanic water to make a comparison with previous studies (C. T. A. Chen et al., 2013; Cotovicz, Knoppers, et al., 2021; Cotovicz, Ribeiro, et al., 2021).

$$k(W92) = 0.31U_{10}^2\left(\frac{Sc}{660}\right)^{-0.5} \quad (5)$$

$$k(W14) = 0.251U_{10}^2\left(\frac{Sc}{660}\right)^{-0.5} \quad (6)$$

Sc is the Schmidt number calculated from in situ temperature and salinity (Wanninkhof, 2014). The hourly wind speed data at the nearest meteorological stations were converted to wind at 10 m after the logarithmic correction $U_{10} = \frac{U_z}{0.097 \times \ln\left(\frac{z}{10}\right) + 1}$, where z is the height of wind sensor above the sea level, and U_z is the measured wind speed (Kremer et al., 2003).

To better understand the high spatial heterogeneity in estuarine air-sea CO_2 exchange, we divided the estuaries into several domains according to the pCO_2 level and the estuarine geometry. Then, we averaged all CO_2 flux measurements within each domain to derive their representative fluxes. Finally, the area-weighted CO_2 flux (F_A) for the entire estuary was calculated by the following equation:

$$F_A = \frac{\sum(F_i \times A_i)}{\sum A_i} \quad (7)$$

where i is the positive integer number, thus F_i and A_i denote the representative CO_2 flux and surface area within domain i.

2.5. Two-Endmember Mixing Model

Considering the overall increasing patterns of concentrations of chemical solutes against salinity, we adopted a two-endmember mixing model to evaluate the carbonate changes and the related biogeochemical activities. The determination of endmember values was described in Text S2 in Supporting Information S1. Using salinity as a conservative tracer, the mixing fractions between river water and seawater for each discrete sample can be calculated by Equations 8 and 9:

$$f_{RI} + f_{SW} = 1 \quad (8)$$

$$S_{RI} \times f_{RI} + S_{SW} \times f_{SW} = S_{meas} \quad (9)$$

S means salinity, f represents the mixing fraction, the subscripts RI and SW indicate the river and seawater endmembers, and meas is the measured value. These fractions were used to predict the conservative concentration of chemical solutes ($[X]_{Mix}$) merely resulting from two endmember mixing:

$$[X]_{Mix} = [X]_{RI} \times f_{RI} + [X]_{SW} \times f_{SW} \quad (10)$$

where X could be DIC, TA, or Ca^{2+}. The total nonconservative concentration of chemical solutes ($\Delta[X]$) is defined as the difference between the measured value and conservative mixing value for which positive means addition and negative means removal:

$$\Delta[X] = [X]_{meas} - [X]_{Mix} \quad (11)$$

2.6. Deviations of DIC and Its Stable Isotope

Regarding DIC composition as an example, the conservative mixing values of DIC and δ^{13}C-DIC are calculated below:

$$DIC_{Mix} = DIC_{RI} \times f_{RI} + DIC_{SW} \times f_{SW} \quad (12)$$

$$\delta^{13}C\text{-}DIC_{Mix} = \frac{\delta^{13}C\text{-}DIC_{RI} \times DIC_{RI} \times f_{RI} + \delta^{13}C\text{-}DIC_{SW} \times DIC_{SW} \times f_{SW}}{DIC_{RI} \times f_{RI} + DIC_{SW} \times f_{SW}} \quad (13)$$

Since the biogeochemical processes that change DIC may have distinct $\delta^{13}C$ sources and isotopic fractionation, it is advantageous to utilize both DIC and $\delta^{13}C$-DIC to distinguish them. Using an approach similar to Alling et al. (2012) and Samanta et al. (2015), the fractional deviations of DIC and $\delta^{13}C$-DIC relative to the conservative mixing values were computed according to the following equations:

$$R_{DIC} = \frac{DIC_{meas} - DIC_{Mix}}{DIC_{Mix}} = \frac{\Delta DIC}{DIC_{Mix}} \quad (14)$$

$$\Delta\delta^{13}C\text{-}DIC = \delta^{13}C\text{-}DIC_{meas} - \delta^{13}C\text{-}DIC_{Mix} \quad (15)$$

The errors of $\Delta[X]$, R_{DIC}, and $\Delta\delta^{13}C$-DIC were propagated from the uncertainties of endmember values and sample measurement according to Taylor's expression (Taylor, 1997). In a plot of $\Delta\delta^{13}C$-DIC against R_{DIC}, the slopes of the vectors that different biogeochemical processes drive the data apart from the origin can be calculated as shown in Text S3 in Supporting Information S1. Note that the data points could be influenced either by one single process (vector) or by multiple processes in sequence (vectors).

2.7. Simulations of pCO_2 and pH

For simplicity, we separated the total nonconservative $[X]$ (DIC or TA) into four components:

$$\Delta[X]_{Total} = \Delta[X]_{AS} + \Delta[X]_{AR} + \Delta[X]_{SR} + \Delta[X]_{CD} \quad (16)$$

where the subscripts AS, AR, SR, and CD denote air-sea CO_2 exchange, aerobic respiration, sulfate reduction, and $CaCO_3$ dissolution, respectively. The amount of nonconservative DIC caused by CO_2 outgassing can be calculated by the equation $\Delta DIC_{AS} = \frac{Flux \times T_f}{H}$, where Flux is the CO_2 flux calculated from pCO_2, T_f means the flushing time, and H is the average water depth. Note that air-sea CO_2 exchange does not affect TA. The apparent oxygen utilization (AOU, the difference between saturated DO and measured DO) was used to estimate the $\Delta[X]_{AR}$ according to the chemical stoichiometry (AOU: $\Delta DIC{:}\Delta TA = 138{:}106{:}(-17)$). Then, the sum of $\Delta[X]_{SR}$ and $\Delta[X]_{CD}$ is calculated as the residue of the above equation and defined as $\Delta[X]^*$ (i.e., ΔDIC^* or ΔTA^*).

$$\Delta DIC^* = \Delta DIC_{Total} - \Delta DIC_{AS} - \Delta DIC_{AR} \quad (17)$$

$$\Delta TA^* = \Delta TA_{Total} - \Delta TA_{AR} \quad (18)$$

Assuming the stoichiometric ratios of $\Delta TA/\Delta DIC$ for SR (1.142) and CD (2) are valid (Cai et al., 2017), we used x and y to represent the quantities of DIC addition via SR and CD, respectively, so the TA changes equal to $1.142x$ for SR and $2y$ for CD.

$$\Delta DIC^* = x + y \quad (19)$$

$$\Delta TA^* = 1.142x + 2y \quad (20)$$

Therefore, the nonconservative DIC and TA contributed by SR and CD can be resolved. To understand how different biogeochemical processes affect pCO_2 and pH in estuarine water, we simulated the pCO_2 and pH dynamics in an accumulative manner based on the evolution of DIC and TA from component processes. Finally, the changes in pCO_2 and pH for each process are defined as the differences between any two sequential curves.

3. Results

3.1. Spatiotemporal Distributions of Surface Water Properties

Tidal movement significantly influences the spatial distributions of physicochemical water parameters in shallow tropical estuaries. In Dongzhai Harbor, the boat departed the wharf just after the low tide (Figure S1a in Supporting Information S1), when the estuarine water went outside farthest away from the estuary. As we went outside to the coastal sea, we observed typical patterns of increasing salinity, DO, pH, and decreasing pCO_2 (Figure 2). When we came back to the estuary entrance (station P12), the water height approached the high tide

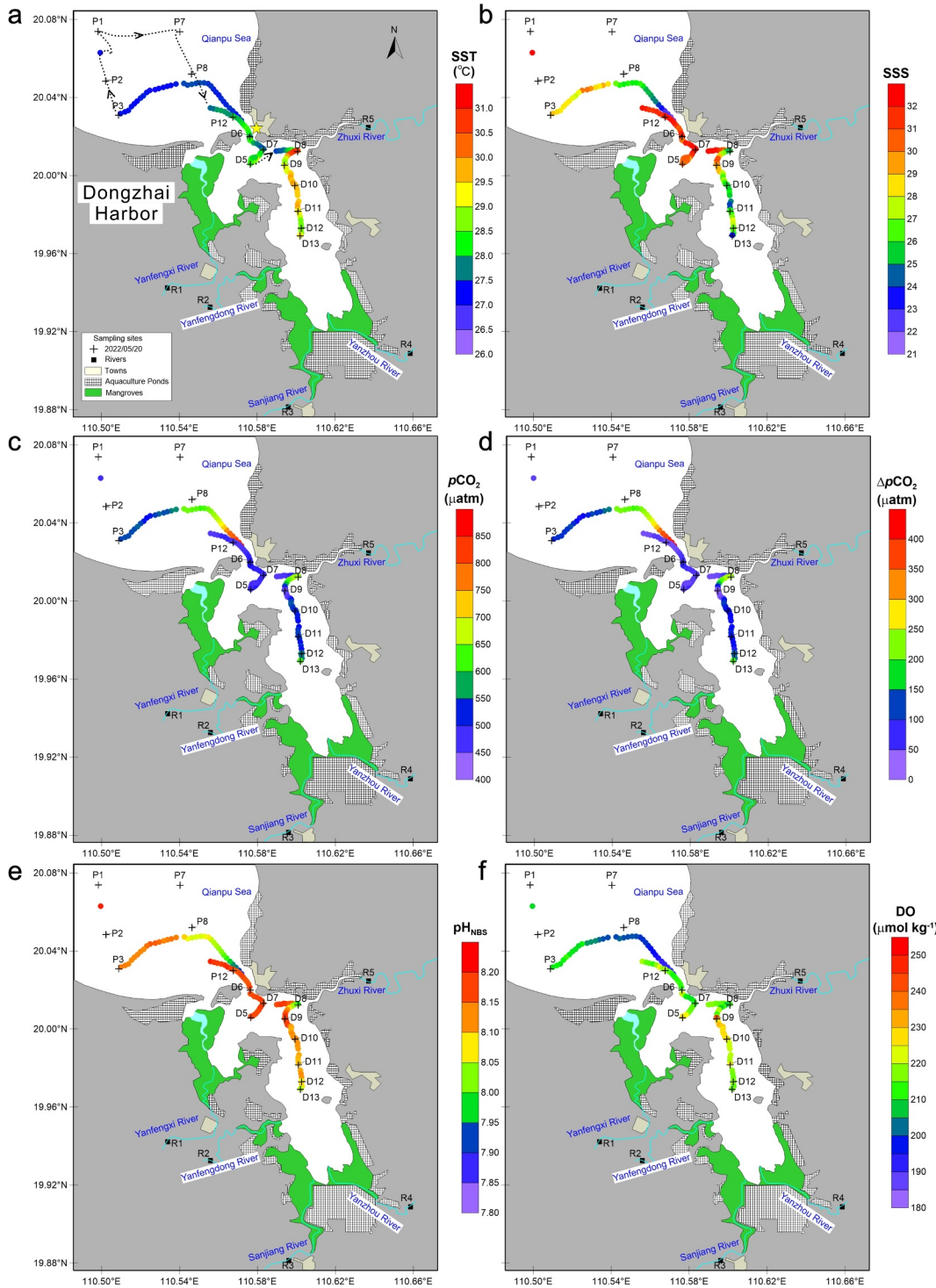

Figure 2. Spatial distributions of surface seawater temperature (SST) (a), salinity (SSS) (b), partial pressure of CO_2 (pCO_2) (c), the difference between observed pCO_2 and atmospheric CO_2 (ΔpCO_2) (d), pH (e), and dissolved oxygen (DO) (f) in the Dongzhai Harbor and the adjacent coastal sea on 20 May 2022. In panel (a), the yellow star shows the starting and ending site during this cruise, whereas the dotted polyline and arrows represent the cruise track where the underway instrument failure occurred.

stage. At the repeated tracks near the estuary entrance, salinity, DO, and pH increased by 42%, 14%, and 3%, respectively, and pCO_2 decreased by 44% due to the intensified seawater intrusion into the estuary. Compared

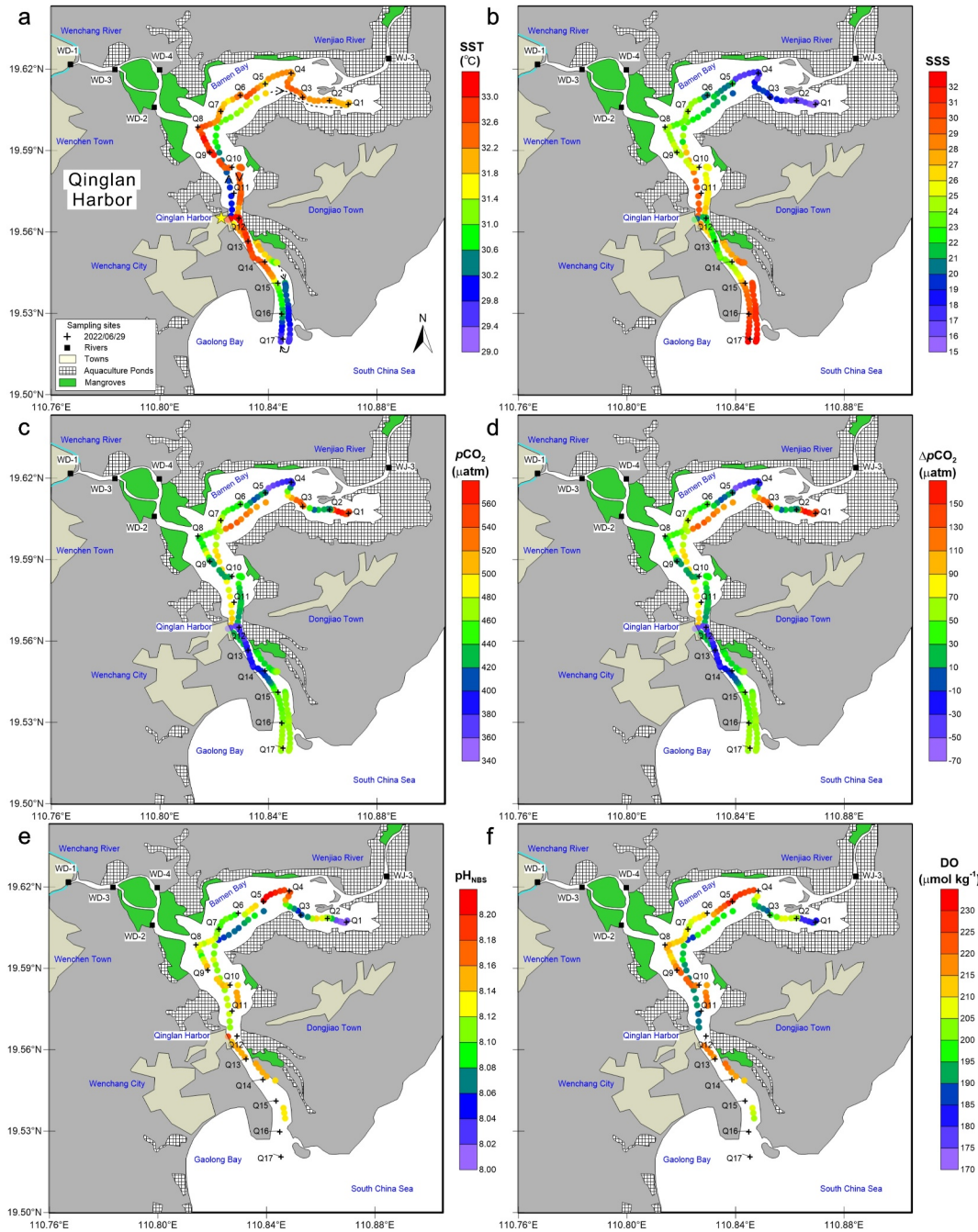

Figure 3. Spatial distributions of SST (a), SSS (b), pCO_2 (c), ΔpCO_2 (d), pH (e), and DO (f) in the Qinglan Harbor on 29 June 2022.

with the signals at the entrance, the medium salinity, slightly lower DO and pH, and slightly higher pCO_2 at the central estuary indicate limited influence from the surrounding rivers during high tide except the site D8 near the mouth of Zhuxi River.

The cruise in Qinglan harbor started at the high tide and ended just before the low tide (Figure S1b in Supporting Information S1). In general, salinity increased from the upper estuary to the coastal sea but varied substantially at the middle estuary due to the stronger interaction of freshwater input and tidal movement (Figure 3b). One of the supports is that the water with low pCO_2 in the northern estuary probably flew toward estuary mouth during ebb tide (Figure 3c) resulting in the decreases of salinity and pCO_2 by 18% and 13%, respectively. The quick changes

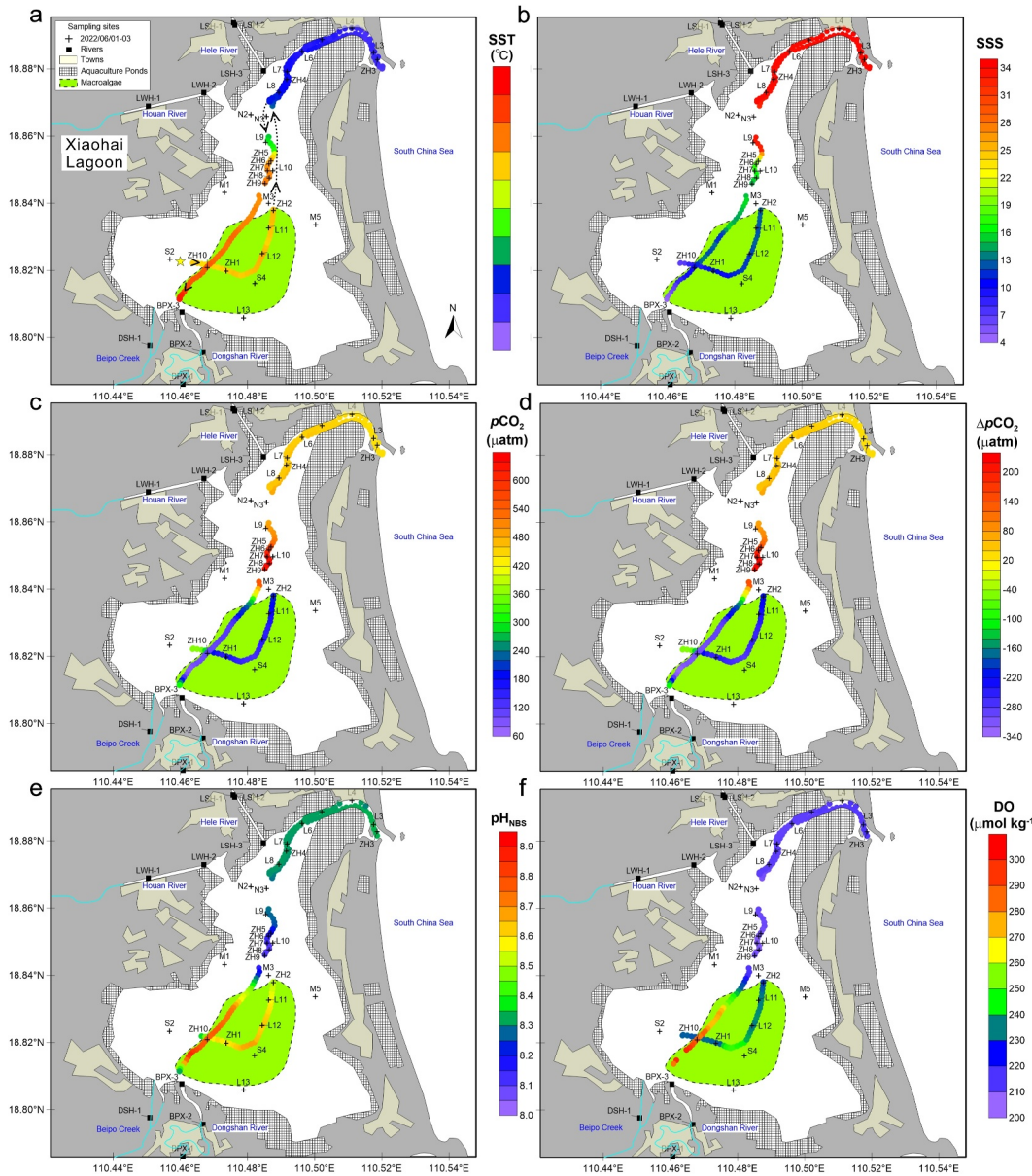

Figure 4. Spatial distributions of SST (a), SSS (b), pCO_2 (c), ΔpCO_2 (d), pH (e), and DO (f) in the Xiaohai Lagoon on 3 June 2022. Note that discrete water samples were taken during June 1–3; however, the underway measurements were performed only on 3 June.

in spatial distributions of water properties represent the high physical and biogeochemical heterogeneities in estuarine regions.

Since the entire sampling campaign was undertaken almost during the high tide (Figure S1c in Supporting Information S1) and the hydrological settings of Xiaohai Lagoon are more confined, the patterns of water properties were generally similar during the forward and backward cruise tracks (Figure 4). Salinity decreased from north to south along with a short transition zone in the middle lagoon, whereas water temperature increased southward. The pCO_2 reached a maximum in the middle lagoon and decreased toward the estuary mouth, where pCO_2 was slightly higher than the atmospheric pCO_2. However, water characterized with low pCO_2 down to 70 μatm, high DO and pH up to 293 μmol kg^{-1} and 8.83 covered a wide region of the southern lagoon, indicating there existed strong photosynthesis, which consumed CO_2 and hydrogen ions to produce oxygen and organic matter.

Table 1
Summary of Calculated Mean ± SD Values for Wind Speed (U_{10}, m s^{-1}), Gas Transfer Velocity (k_{600}, cm hr^{-1}), and Air-Sea CO_2 Flux (mmol m^{-2} d^{-1}) in Each Estuary

	Dongzhai Harbor			Qinglan Harbor			Xiaohai Lagoon		
Parameterizations	U_{10}	k_{600}	Flux	U_{10}	k_{600}	Flux	U_{10}	k_{600}	Flux
W92[a]	2.1 ± 1.2	2.0 ± 1.5	0.8 ± 0.5	2.6 ± 0.2	2.2 ± 0.4	0.7 ± 0.2	4.4 ± 0.9	6.6 ± 2.6	−3.8 ± 4.9
W14[a]		1.6 ± 1.2	0.7 ± 0.4		1.8 ± 0.3	0.6 ± 0.2		5.4 ± 2.1	−3.1 ± 4.0
RC01		4.4 ± 1.6	3.3 ± 1.7		4.7 ± 0.3	1.6 ± 0.4		9.5 ± 3.0	−5.8 ± 5.8
B04		6.5 ± 3.2	3.8 ± 2.7		7.7 ± 0.5	2.6 ± 0.7		12.4 ± 2.4	−8.1 ± 5.3
J08		5.0 ± 0.9	4.8 ± 2.2		5.0 ± 0.3	1.7 ± 0.5		8.5 ± 2.2	−5.4 ± 4.4

[a]The conversion from k_{660} to k_{600} needs a multiplication of 1.049 assuming the dependence of gas transfer velocity on Schmidt number scales to $Sc^{-0.5}$.

3.2. Air-Sea CO_2 Flux

According to the air-sea pCO_2 gradients (Table S1 in Supporting Information S1), most of the area of the two mangrove estuaries are net sources to the atmospheric CO_2, whereas the lagoon generally behaves as a CO_2 sink. The average wind speed in Xiaohai Lagoon (4.4 m s^{-1}) is nearly twice as high as that in mangrove estuaries (2.1–2.6 m s^{-1}) (Table 1). The average gas transfer velocities estimated by estuarine models (4.4–12.4 cm hr^{-1}) are comparable to previous studies (Rosentreter et al., 2018) and are significantly higher than that estimated by oceanic parameterizations (1.6–6.6 cm hr^{-1}). Therefore, we take the average of the fluxes estimated by the three estuarine models (RC01, B04, and J08) to represent the air-sea CO_2 fluxes in the three estuaries. The CO_2 emission in Dongzhai Harbor (4.0 ± 1.3 mmol m^{-2} d^{-1}) is twice higher than that in Qinglan Harbor (2.0 ± 0.3 mmol m^{-2} d^{-1}), whereas the magnitude of CO_2 sink in Xiaohai Lagoon is 6.4 ± 3.0 mmol m^{-2} d^{-1}.

3.3. Carbonate Dynamics in the Water Column

Significant vertical gradients of salinity (>3) were only observed close to the river mouth (e.g., D10-11, Q6-7) or in the deep channel (e.g., Q9-11), indicating that most of the water column was thoroughly mixed across the three shallow tropical estuaries. The ranges of DIC and TA in the river end were generally larger than that in the seawater end along with an increasing pattern different from the linear line (Figure 5) especially in Qinglan Harbor and Xiaohai Lagoon, suggesting nonconservative behaviors driven by external inputs or internal biogeochemical activities (Cai & Wang, 1998).

To evaluate the carbonate dynamics over an estuary-wide scale, we applied a two-endmember mixing scheme between river water and offshore seawater (Table 2). In Dongzhai Harbor, moderate additions of DIC (25.6–92.6 μmol kg^{-1}) and TA (−5.3–76.6 μmol kg^{-1}) were observed in the high salinity region (Figure 6a). In Qinglan Harbor, both ΔDIC and ΔTA reached a peak (256.5 and 359.1 μmol kg^{-1}) at salinity ∼8 and decreased to zero toward river and ocean ends (Figure 6b). In Xiaohai Lagoon, DIC and TA were moderately added in the northern lagoon but strongly removed in the southern lagoon (Figure 6c). Note that the removal of DIC (<301.4 μmol kg^{-1}) is much larger than TA (<90.6 μmol kg^{-1}) in the southern lagoon, which is quite different from the two mangrove estuaries. For the two mangrove estuaries, the ratio of ΔTA/ΔDIC significantly increased from inside (0.67) to outside (1.96) Dongzhai Harbor (Figure 6d) while it kept consistent (1.50) throughout the Qinglan Harbor (Figure 6e). The ratio of ΔTA/ΔDIC in the northern Xiaohai Lagoon (0.72) is close to that inside Dongzhai Harbor but is significantly larger than that in the southern lagoon (0.24 on June 1, 0.29 on June 3) (Figure 6f).

The δ^{13}C-DIC in three tropical estuaries generally fall within the ranges of that in a large subtropical estuary, that is, the Pearl River Estuary (J. Su et al., 2017) but show some systematic differences probably due to different natural and anthropogenic forcings in each estuarine system (Figures 7a–7c). All the observed Ca^{2+} concentrations are lower than those in the northern South China Sea shelf water (Cao et al., 2011) (Figures 7d–7f), indicating that the physical and biogeochemical controls on Ca^{2+} dynamics are more complex and intensive in the estuary than in the shelf.

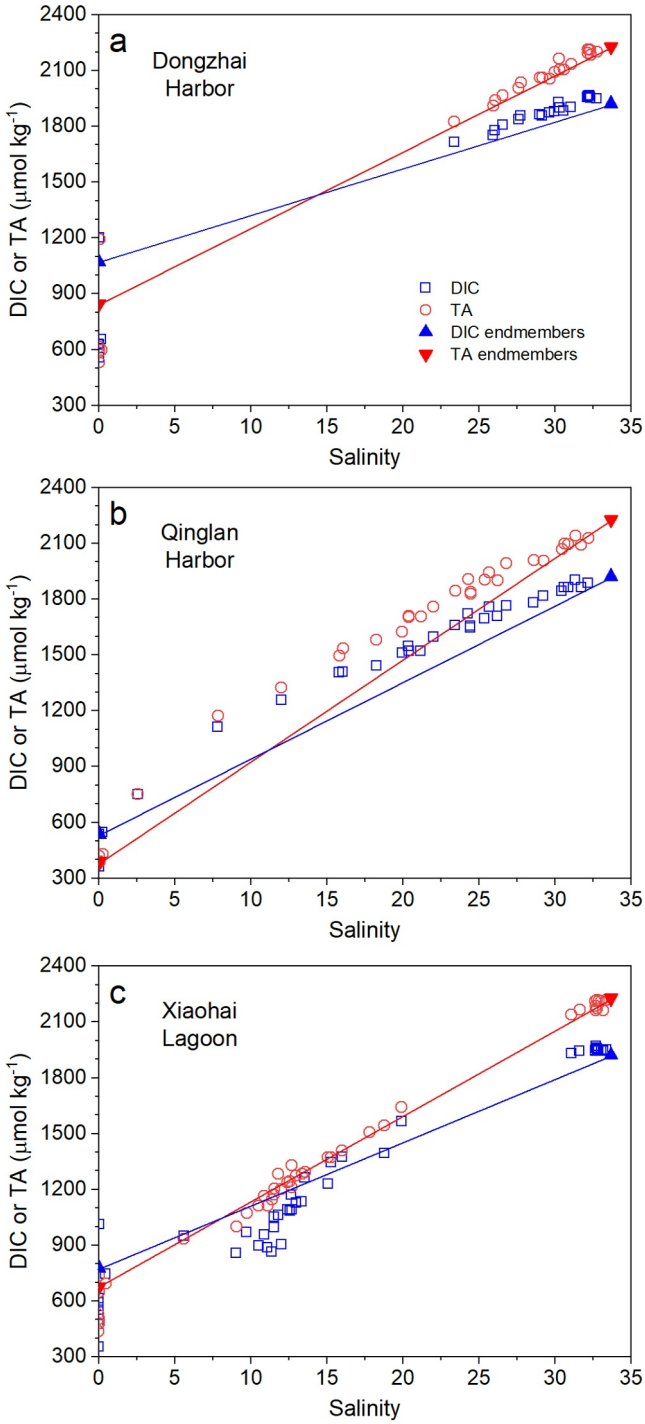

Figure 5. Distributions of DIC and TA against salinity in Dongzhai Harbor (a), Qinglan Harbor (b), and Xiaohai Lagoon (c). The two endmembers (solid triangles) were used to derive the conservative mixing lines (solid lines).

In mangrove estuaries, the majority of the deviations of DIC concentration (R_{DIC}) and δ^{13}C-DIC lie on the fourth quadrant, whereas part of the data fall onto the first quadrant, suggesting the functioning of organic matter degradation and $CaCO_3$ related processes (Figures 8a and 8b). With a smaller magnitude, the data in northern Xiaohai Lagoon distribute in a similar pattern with Qinglan Harbor (Figure 8c). However, the data in southern lagoon lie on the second quadrant, indicating the involvement of primary production and $CaCO_3$ formation. The CO_2 outgassing is excluded as the southern lagoon acted as a strong sink for atmospheric CO_2. Relative to the conservative mixing lines, both the addition (positive value) and removal (negative value) of Ca^{2+} (ΔCa^{2+}) can be found in the three estuaries, though they occurred in different salinity domains with different magnitudes (Figures 8d–8f).

4. Discussion

The metabolic activities and the related biogeochemistry in blue carbon ecosystems can influence the carbonate dynamics of the coastal zone. For instance, the anaerobic respiration in mangrove sediments can produce more TA than DIC (Saderne et al., 2021; Sippo et al., 2016), which can be exported to the adjacent estuaries/coastal sea via tidal pumping (X. Chen et al., 2018; Faber et al., 2014; Maher et al., 2013). Effective CO_2 outgassing within the mangrove creek increases the content of carbonate ions ($[CO_3^{2-}] \approx$ [TA-DIC]) outwelled to the coastal water (X. Chen et al., 2021; L. Xue & Cai, 2020). The strong photosynthesis coupled with $CaCO_3$ formation can decrease both DIC and TA within seagrass beds (J. Su, Cai, Brodeur, Chen, et al., 2020). The changes in DIC and TA could be transferred to the variations in pCO_2 and pH and be quantified via the program CO2SYS. In the following sections, we estimated the air-sea CO_2 fluxes in each estuary, applied multiple approaches to constrain the major controls on the carbonate system, and quantified how each biogeochemical process affects coastal pCO_2 and pH.

4.1. CO_2 Emission in Mangrove Estuaries and Uptake in a Tropical Lagoon

The air-sea CO_2 flux in estuarine waters is highly variable in different spatial and temporal scales (Maher et al., 2015), which is evidenced by the range of ΔpCO_2 (−271~182 μatm) in different domains of the three estuaries (Table S1 in Supporting Information S1), and the distinct water properties in the revisited cruise track at different tidal stages (Figures 2 and 3). Through calculating the area-weighted CO_2 flux rather than simply taking the average of the whole data set, we can know more about the status of atmospheric CO_2 source/sink in each estuarine domain and finally get a flux number more representative to the entire estuary (Guo et al., 2009). Another uncertainty in estimating CO_2 flux stems from the application of different gas transfer velocity models. Previous studies have demonstrated that in addition to wind speed, the current generated turbulence may become the main driver controlling k and enhance the air-sea exchange rate in shallow coastal waters (Rosentreter et al., 2017). Due to the lack of the current velocity data, we utilized multiple wind-k models to constrain the estuarine CO_2 flux and found that the k estimated by estuarine parameterizations were significantly higher than that calculated by oceanic parameterizations especially when the wind speed is low (Table 1). Although the estimated estuarine k fall within the previous studies (Ho et al., 2014; Jiang et al., 2008; Rosentreter et al., 2017, 2018), the measurements of site-specific k is recommended in the highly dynamic tidal estuarine ecosystems.

Table 2
Summary of Endmember Values of Salinity, DIC, TA, Ca^{2+}, δ^{13}C-DIC, and Their Uncertainties

Endmembers	Regions	Salinity (psu)	DIC (μmol kg^{-1})	TA (μmol kg^{-1})	Ca^{2+} (μmol kg^{-1})	δ^{13}C-DIC (‰)
Riverine	Dongzhai Harbor	0.00	1070.8 (±41.9)[a]	844.6 (±50.9)[a]	196 (±5)	−10.2 (±0.1)
	Qinglan Harbor	0.05 (±0.01)	536.1 (±2.0)	388.2 (±2.0)	136 (±5)	−14.2 (±0.1)
	Xiaohai Lagoon	0.00	776.7 (±23.8)[a]	674.7 (±18.2)[a]	482 (±5)	−12.6 (±0.1)
Offshore	Dongzhai Harbor	33.67 (±0.07)[b]	1921.8 (±9.2)[b]	2227.0 (±7.4)[b]	9553 (±5)	−0.9 (±0.1)
	Qinglan Harbor	33.67 (±0.07)	1921.8 (±9.2)	2227.0 (±7.4)	9474 (±5)	−1.1 (±0.1)
	Xiaohai Lagoon	33.67 (±0.07)	1921.8 (±9.2)	2227.0 (±7.4)	9439 (±5)	−0.2 (±0.1)

[a]The discharge-weighted composite river endmembers were derived from the effective concentration method (see Text S2 in Supporting Information S1). [b]Cited from Guo and Wong (2015).

The area-weighted mean CO_2 emission rate to the atmosphere was 2.0–4.0 mmol m^{-2} d^{-1} in the two mangrove estuaries. This result is much lower than the global mean CO_2 flux density (43–72 mmol m^{-2} d^{-1}) in mangrove waters (Rosentreter et al., 2018). Also, it is about one order of magnitude lower than the median CO_2 flux density (~30 mmol m^{-2} d^{-1}) of the tidal systems/deltas in the East Asia. The lower CO_2 fluxes in Dongzhai Harbor and Qinglan Harbor can be attributed to (a) that the study sites are more representative of marine systems with a smaller air-sea gradients of pCO_2 relative to other mangrove waters (Call et al., 2015), and (b) that the gas transfer velocity may be underestimated by the estuarine parameterizations solely based on wind speed (Ho et al., 2014, 2016), and (c) that the wind speed was relatively low during cruises (Jiang et al., 2008).

In a most recent review, global lagoons account for 25% of the surface areas in estuaries and generally behave as a CO_2 source to the atmosphere with a global median CO_2 flux density of 16.1 mmol m^{-2} d^{-1} (Rosentreter et al., 2023). The area-weighted mean CO_2 flux was −6.4 mmol m^{-2} d^{-1} in Xiaohai Lagoon. The magnitude of CO_2 flux is about one third of global median value with an opposite direction for gas exchange. However, this rate is comparable to the oligohaline Aby Lagoon of Ivory Coast (West Africa) with an annual CO_2 sink of −7.4 mmol m^{-2} d^{-1} (Koné et al., 2009), three geomorphically distinct autotrophic Australian estuaries with an annual CO_2 flux density range of −1.1 ~ −5.5 mmol m^{-2} d^{-1} (Maher & Eyre, 2012), and the eutrophic hypersaline Araruama Lagoon (Southeast Brazil) with an annual CO_2 sink of −7.6 ~ −10.4 mmol m^{-2} d^{-1} (Cotovicz, Knoppers, et al., 2021). It's essential to include the CO_2 sinks of autotrophic lagoons/estuaries in global estimate of the estuarine air-sea CO_2 flux, otherwise, the flux may be over-estimated.

4.2. Biogeochemical Drivers of TA and DIC Dynamics

The chemical stoichiometry either between the salinity normalized TA and DIC (Reithmaier et al., 2020; Rosentreter & Eyre, 2025; Santos et al., 2019; Sippo et al., 2016) or between the nonconservative TA and DIC (ΔTA/ΔDIC) (Cabral et al., 2021; Cotovicz, Ribeiro, et al., 2021; Thibault de Chanvalon et al., 2023) is widely used to uncover the biogeochemical drivers of TA and DIC dynamics in the coastal environments especially the mangrove tidal creeks and estuaries. This stoichiometric ratio is a combined result of different pathways of organic matter remineralization, which have specific slope values (e.g., aerobic respiration (AR) = −0.16, denitrification = 0.94, MnO_2 reduction = 4.14, FeOOH reduction = 8.14, and sulfate reduction (SR) = 1.14) (Cai et al., 2010). Also, the formation or dissolution of $CaCO_3$ can remove or add TA and DIC with a ratio of 2. To overcome the limitation of this stoichiometric method (Yin et al., 2024), we incorporate many other parameters to acquire a more robust understanding of the biogeochemical controls on TA and DIC.

4.2.1. Dongzhai Harbor

In Dongzhai Harbor, the mild oxygen deficit (<30 μmol kg^{-1}) and pCO_2 oversaturation (<200%) suggest the small contribution of aerobic respiration and CO_2 outgassing to the changes of carbonate system. Due to the abundance of seawater sulfate and the high organic matter content in mangrove sediment, sulfate reduction is usually the dominant anaerobic respiration pathway for TA and DIC production, assuming that part of the sulfide is trapped in the sediment as pyrite (Borges et al., 2003; Bouillon et al., 2007; Reithmaier et al., 2021). The additions of TA and DIC and their ratio (0.67) inside Dongzhai Harbor indicate the involvement of aerobic respiration and sulfate reduction (Figures 6a and 6d). Moreover, the majority of the deviations of DIC

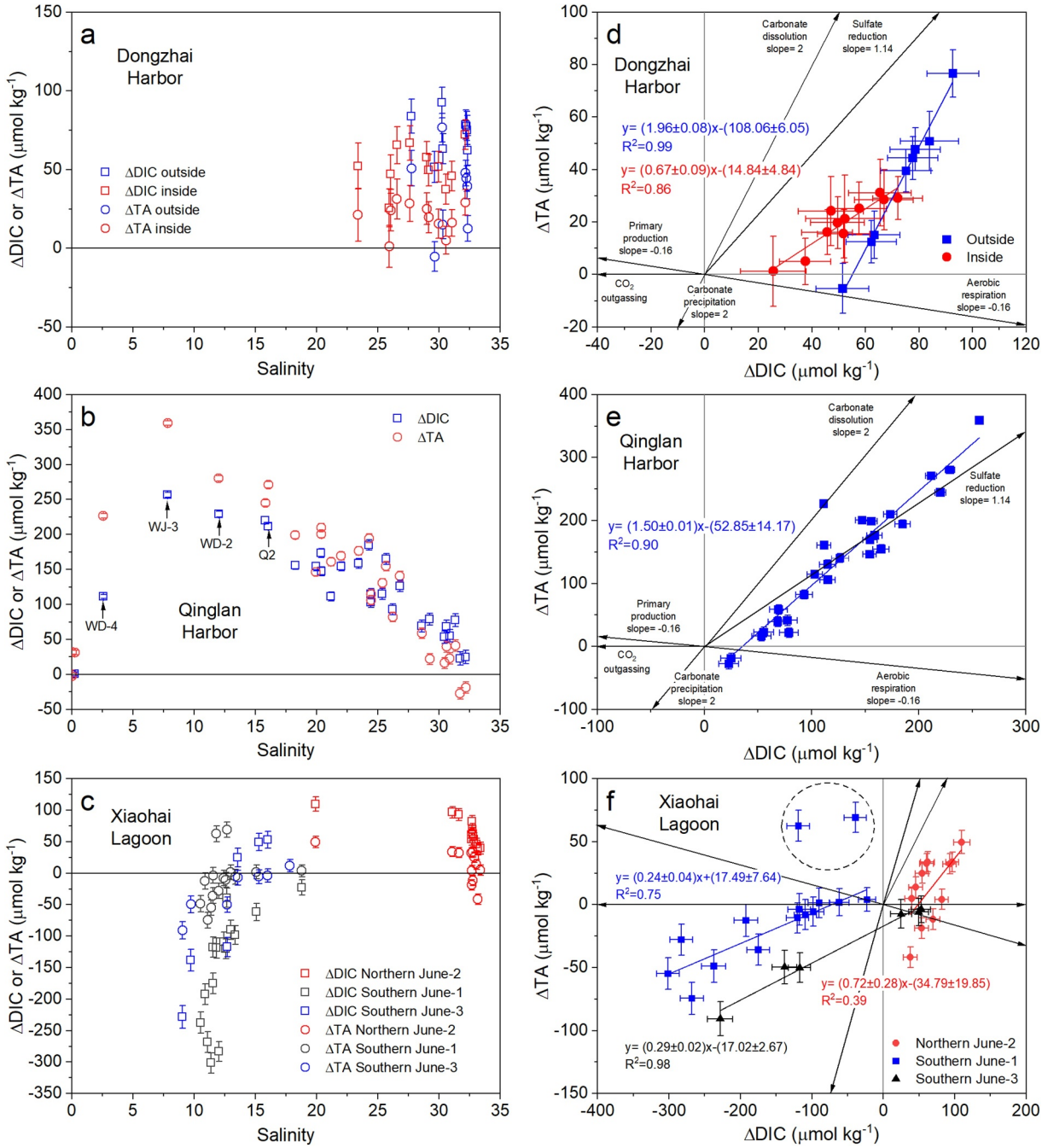

Figure 6. Distributions of nonconservative DIC and TA against salinity (a–c) and their ratios (d–f). Note that in panel (f), the space is too crowded to add the names of processes, which can be referred to panels (d) and (e) in a similar order. Two data points inside the dashed circle are not included in the linear regression. The errors of ΔDIC and ΔTA were propagated from the uncertainties of endmember values and sample measurement according to Taylor's expression (Taylor, 1997).

concentration (R_{DIC}) and δ^{13}C-DIC in Dongzhai Harbor lie on the fourth quadrant (Figure 8a), which can be seen as the combined results of aerobic respiration and sulfate reduction. Previous studies indicate that minor or no isotopic fractionation occurs during these two degradation pathways (J. Su, Cai, Brodeur, Hussain, et al., 2020). Therefore, these two processes would share the same vectors and cannot be differentiated.

The data on the left and right sides of the degradation vectors suggest that $CaCO_3$ precipitation and dissolution may occur, which is confirmed with the positive and negative nonconservative Ca^{2+} (Figure 8d). The Ca^{2+} additions probably stem from carbonate dissolution in the high organic content mangrove sediments, where the

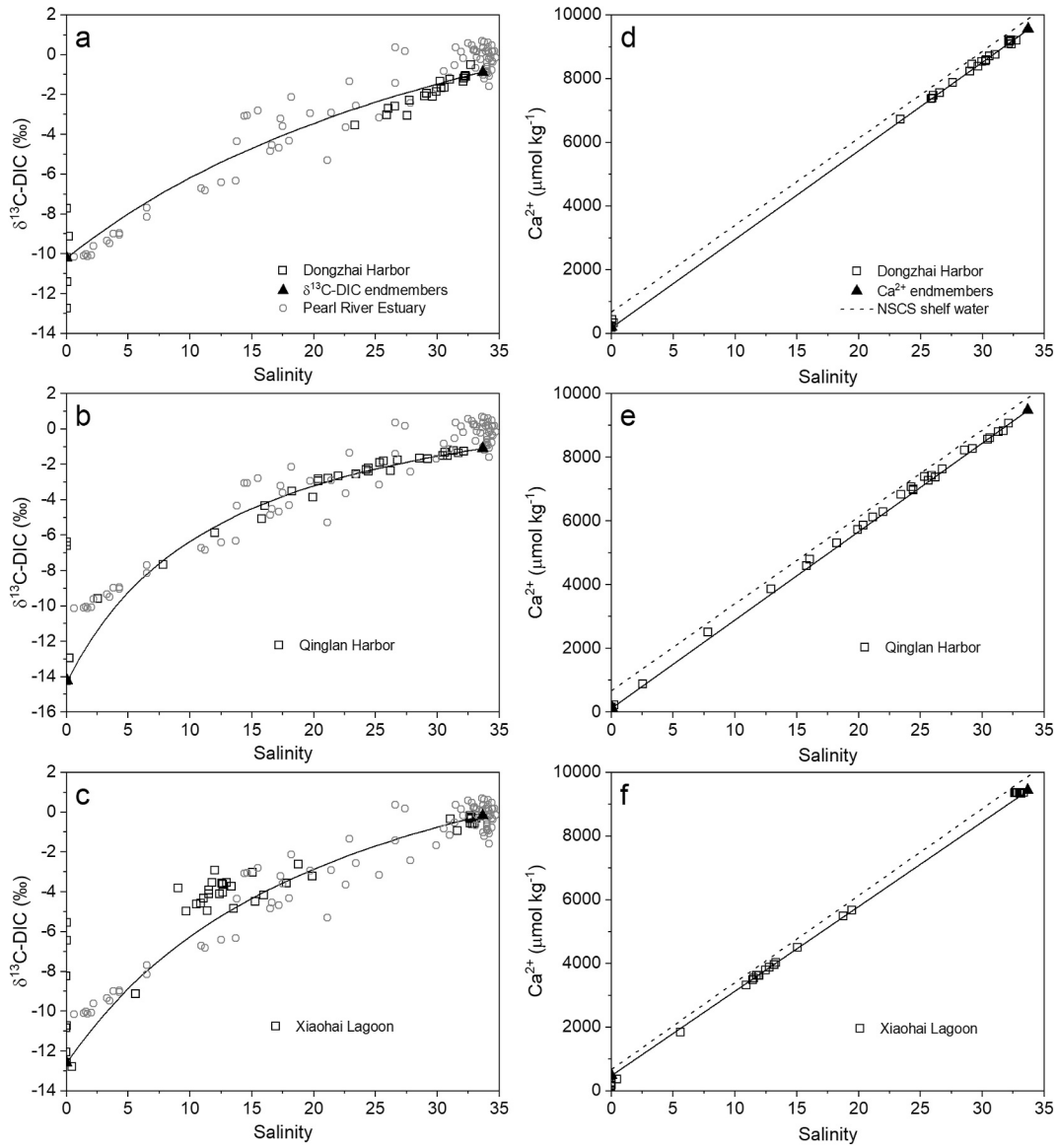

Figure 7. Distributions of δ^{13}C-DIC (a–c) and Ca^{2+} concentration (d–f) against salinity. The solid curves indicate the conservative mixing lines between river water and offshore seawater. Cited from J. Su et al. (2017), the gray open circles are δ^{13}C-DIC data collected in the lower reach of Pearl River Estuary and the adjacent coastal sea in July 2014. As a reference, the dashed line represents the Ca^{2+}-salinity relationships ($Ca^{2+} = 273 \times \text{Salinity} + 675$, $n = 163$, $r = 0.99$) for the northern South China Sea shelf waters cited from Cao et al. (2011).

CO_2 and acids produced by aerobic and anaerobic respiration can promote the dissolution of $CaCO_3$ (Reithmaier et al., 2023). However, Ca^{2+} removal may reflect the perturbations from human aquaculture activity, because the intertidal zone of Dongzhai Harbor is an important mariculture base for bivalves and the growth of shells would consume Ca^{2+}. The ratio of $\Delta TA/\Delta DIC$ significantly increased outside Dongzhai Harbor (1.96) because estuarine water flew in a clockwise direction that went through the mangroves located in the southern and western estuary and finally arrived in the adjacent coastal sea, and mangroves could export more TA than DIC to the nearby water body via tidal pumping (Sippo et al., 2016). The higher $\Delta TA/\Delta DIC$ ratio may reflect additional contribution from metal oxide reductions (Kristensen et al., 2000).

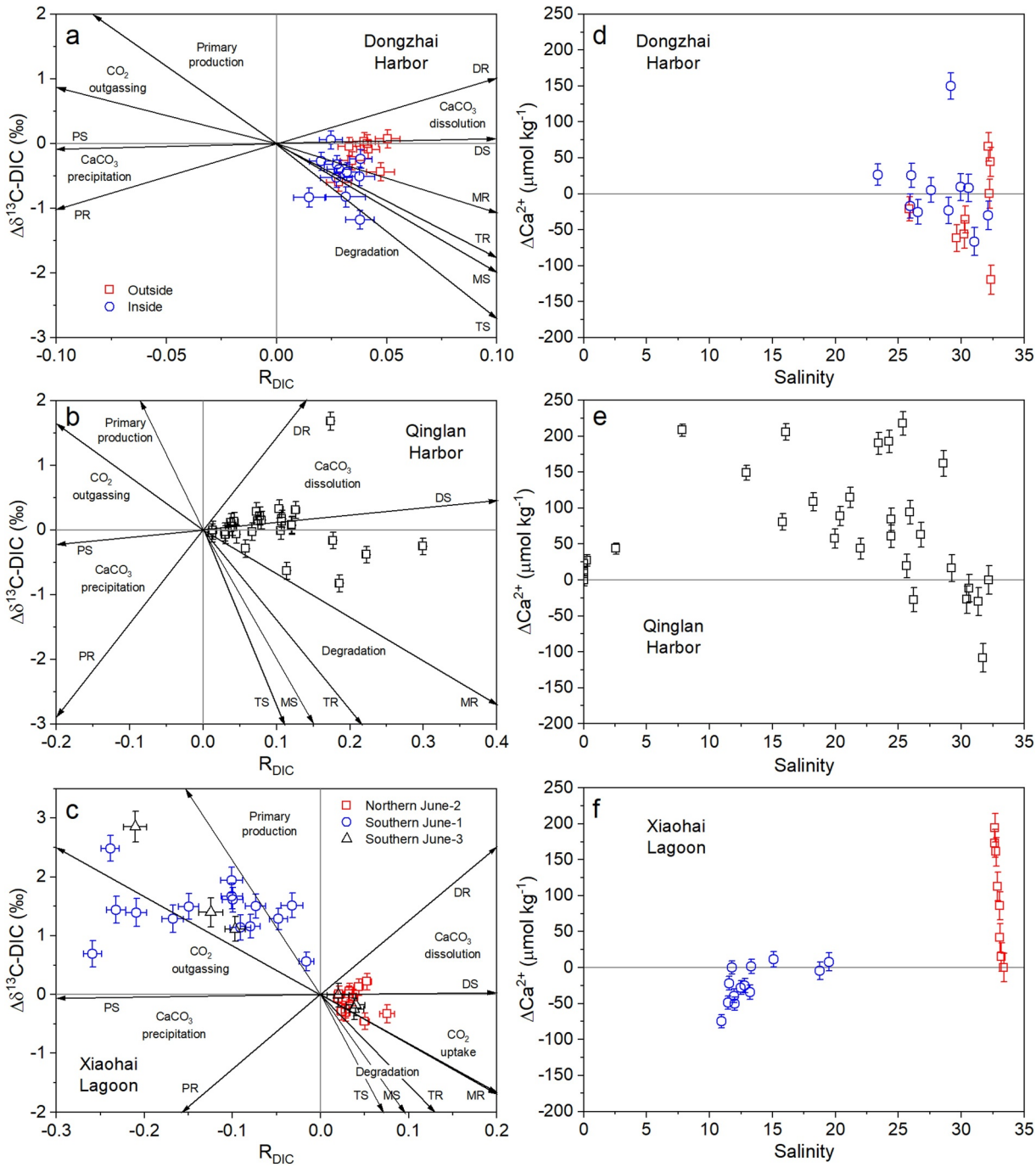

Figure 8. Deviations of δ^{13}C-DIC and concentrations of DIC (a–c) and Ca^{2+} (d–f) relative to their respective conservative mixing lines. The origins in panels (a–c) indicate the data only controlled by the conservative mixing. The four vectors (TS, TR, MS, and MR) indicate the effects of degradation of organic carbon, which are determined by the sources of organic carbon (T: terrestrial source; M: marine source) and the initial DIC and δ^{13}C-DIC composition in the water (S: seawater; R: river water). The four vectors (DS, DR, PS, and PR) denote the dynamic change of $CaCO_3$ mineral (D: dissolution; P: precipitation), which depend on the δ^{13}C of $CaCO_3$ and the δ^{13}C-DIC of seawater (S) and river water (R). In panels (d–f), positive means addition while negative indicates removal of Ca^{2+}. The errors of $\Delta\delta^{13}$C-DIC, R_{DIC}, and ΔCa^{2+} were propagated from the uncertainties of endmember values and sample measurement according to Taylor's expression (Taylor, 1997).

4.2.2. Qinglan Harbor

Also as a mangrove estuary, Qinglan Harbor has larger additions of TA and DIC but a lower ΔTA/ΔDIC ratio (1.50) compared with that outside Dongzhai Harbor (1.96) (Figures 6b and 6e). Nearly half of the data ($\Delta\delta^{13}$C-

DIC vs. R_{DIC}) fall within the area between organic matter degradation and carbonate dissolution, and the other half lies in the area of carbonate dissolution, indicating the role of carbonate dissolution may surpass aerobic respiration or sulfate reduction (Figure 8b). The ΔCa^{2+} was minor in the river and ocean ends but reached peak value around salinity 8 (Figure 8e). The co-occurrence of large additions of Ca^{2+}, DIC, and TA as well as ^{226}Ra (N. Su et al., 2011), near the river mouths surrounding by mangroves (i.e., stations Q8, WJ-3, and Q2) indicates that submarine groundwater discharge or porewater exchange plays an important role in delivering the chemical solutes within mangrove sediments to the estuary (Saderne et al., 2021; Sippo et al., 2016). Given the high percentage of fine particles ((clay + silt)% equals to 35%–94%) in Qinglan mangrove sediments (Bao et al., 2013), the fresh groundwater discharge from the land side would be minor due to the low permeability, whereas recirculated seawater discharge to the seaside might dominate because of the ubiquitous animal burrows in mangrove sediments (X. Chen et al., 2018; Santos et al., 2012). By increasing the sediment-water interface area, the burrows can not only enhance the remineralization of organic matter and the release of nutrients and metals but also facilitate sediment-water exchange through multiple physical drivers such as bioirrigation and convective transport (Tait et al., 2016). Unlike the previous studies (N. Su et al., 2011; Wu et al., 2021), we focus more on carbonate dynamics of estuarine waters, thus characterizing the chemical solutes of porewater or groundwater and quantifying their specific fluxes are beyond the scope of our study.

A recent study has demonstrated that restoring mangroves can trap carbonate from elsewhere (i.e., allochthonous carbonates) resulting in high-carbonate-content sediments, where alkalinity production is enhanced by the increased rates of anaerobic respiration (e.g., sulfate reduction) and $CaCO_3$ dissolution (Fakhraee et al., 2023). Considering fringing coral reefs grow a few hundred meters off Qinglan Harbor and abundant debris of coral skeleton are seen on a beach ~5 km southwest to the mouth of Qinglan Harbor, the carbonate content of mangrove sediments should be high enough to support the strong carbonate dissolution there. Therefore, we speculate that at least four processes including aerobic respiration, CO_2 outgassing, carbonate dissolution, and sulfate reduction contribute to the changes of TA and DIC (Reithmaier et al., 2023), and data simulations were made to decompose the fractions from multiple processes later (see Section 4.3).

4.2.3. Xiaohai Lagoon

In the northern Xiaohai Lagoon, the ratio of $\Delta TA/\Delta DIC$ (0.72) is close to that inside Dongzhai Harbor (0.67) (Figures 6d and 6f), and the majority of the data ($\Delta\delta^{13}C$-DIC vs. R_{DIC}) lie on Quadrant 4 (Figure 8c), indicating a combined effect of organic matter degradation and carbonate dissolution. The ΔCa^{2+} reached a maximum value (194 μmol kg^{-1}) at station L5 around salinity 32.7 and decreased abruptly toward the lagoon mouth (33.4). Similar decreasing trends within such a narrow salinity range were also found for ΔDIC and ΔTA with much smaller ranges (38–93 and 5–34 μmol kg^{-1}, respectively), indicating limited $CaCO_3$ dissolution occurred there. The large excess Ca^{2+} could come from the other source, anthropogenic $CaCl_2$, which is prevalent in ice-making, defogging, and dust control in fishery harbors with dense human populations. There are three ice-making plants ~5 km to the northwest of station L5, suggesting that the anthropogenic perturbation could be significant at a local scale.

In the southern lagoon, the significant removal of TA and DIC and their ratio (0.24 on June 1, 0.29 on June 3) suggest the possible involvement of primary production and $CaCO_3$ formation (Figures 6c and 6f). The majority of data ($\Delta\delta^{13}C$-DIC vs. R_{DIC}) fall onto Quadrant 2 (Figure 8c), indicating that primary production plus carbonate formation rather than CO_2 outgassing are the main controls of DIC and $\delta^{13}C$-DIC. Furthermore, the extremely low pCO_2, high DO, and pH confirm strong photosynthesis driven by macroalgae beds (Figures 4c–4f), whereas the removal of Ca^{2+} and the relatively high $CaCO_3$ saturation index ($\Omega_{calcite} > 3.0$) confirm the occurrence of $CaCO_3$ formation (Figure 8f). This phenomenon is also found in a eutrophic hypersaline lagoon, where the CO_2 uptake by phytoplankton photosynthesis accounts for ~60% of DIC reduction, whereas the remaining is attributed to $CaCO_3$ precipitation (Cotovicz, Knoppers, et al., 2021). Previous studies have demonstrated that photosynthesis-induced high-pH and high-Ω conditions could enhance biogenic calcification and abiotic $CaCO_3$ precipitation within the submerged aquatic vegetation beds (Enríquez & Schubert, 2014; J. Su, Cai, Brodeur, Chen, et al., 2020).

4.3. Evolution of CO_2 Flux and Coastal Acidification Along the Salinity Gradient

To quantify how blue carbon ecosystems modulate the air-sea CO_2 flux (i.e., pCO_2) and coastal acidification (i.e., pH) in tropical estuaries, we choose Qinglan Harbor as an example because it suffers from minor anthropogenic influence but significant material export from mangroves during the estuarine mixing. Assumptions are made to simplify the simulations of carbonate parameters. First, we adopt the existing two-endmember mixing scheme in Qinglan Harbor as a baseline. Second, we force the total nonconservative DIC and TA to peak at salinity 8 (257 μmol kg^{-1} for ΔDIC_{Total} and 359 μmol kg^{-1} for ΔTA_{Total}) and decrease to zero toward river and ocean ends as we observed. Third, we set the changes of TA and DIC induced by air-sea CO_2 exchange and aerobic respiration as constants throughout the estuary.

Although there is a high spatial heterogeneity in CO_2 oversaturation and DO deficit in Qianlan Harbor, they only alter small amount of TA and DIC over the entire estuary. Given the estuary-wide CO_2 flux is 2.0 mmol m^{-2} d^{-1}, the flushing time is 3.9 days (N. Su et al., 2011), and the mean water depth (H) is 1.0 m, the amount of DIC altered by CO_2 emission could be computed by $\Delta DIC_{AS} = \frac{Flux \times T_f}{H} = -7.7$ μmol kg^{-1}, which is ∼0.5% of the estuarine DIC (Figure 5b). The result is consistent with previous studies that the maximum quantity associated with CO_2 evasion was only 0.2–1% for DIC and 0.08–0.1‰ for δ^{13}C-DIC in mangrove tidal creeks (Maher et al., 2013; Taillardat et al., 2018). Furthermore, the theoretical DIC concentrations in equilibrium with the atmosphere at measured temperatures, salinities, TA, and pCO_2 at 410 μatm were on average 1.3% lower than the measured DIC, which is comparable to the reduction percentage of 5% in an Australian mangrove tidal creek (Santos et al., 2019). Note that air-sea CO_2 exchange did not affect TA.

Compared with stratified deep water, the relatively quick replenishment of oxygen in shallow water would underestimate the rate of aerobic respiration based on AOU. Therefore, we set the estuarine-wide mean AOU as 30 μmol kg^{-1} twice the amount of the upper limit of observed AOU. Thus, the amounts of DIC and TA changed by aerobic respiration (i.e., DIC_{AR} and TA_{AR}) equal to 23.0 (∼9% of maximum ΔDIC_{Total}) and −3.7 (∼−1% of maximum ΔTA_{Total}) μmol kg^{-1}. Note that our purpose of smoothing out the changes of DIC and TA driven by AS and AR is to emphasize the dynamics of SR and CD along the salinity gradient, and adjusting the times of observed AOU within a reasonable range would not change the distribution patterns of DIC_{SR}, TA_{SR}, DIC_{CD}, and TA_{CD} against salinity.

Since both SR and CD produce DIC and TA, only positive solutions of Equations 19 and 20 at a salinity range of 2–29 are presented in Figure S3 in Supporting Information S1. As expected, the additions of DIC and TA reach peak values at salinity 8 and decrease toward river and seawater ends. The amount of DIC changes by SR only exceeds that by CD at a salinity range of 5–18. As SR declines faster than CD, its percentage contributions to ΔDIC* and ΔTA* decrease from 58.2% and 44.3% to 0.4% and 0.2%. As the dominant process producing TA, CD substantially increased the acid-buffering capacity of the estuarine water.

The underway data and those calculated from observed DIC and TA data are in good accordance with the simulated curves of pCO_2 and pH (Figures 9a and 9b), supporting that our simplified assumptions and simulations are reasonable. AR is the only process increasing pCO_2 and decreasing pH because it produces CO_2 and acid (Figures 9c and 9d). With constant DIC addition and TA removal from AR, ΔpCO_2 reaches a maximum at low salinity and decreases toward higher salinity, whereas pH reduction reaches a maximum around salinity 11 and decreases toward lower and higher salinity. A low rate of CO_2 evasion results in very minor pCO_2 reduction and pH increment. Although the changes of DIC and TA induced by SR are much larger than that by AR (Figures S3a and S3b in Supporting Information S1), its impacts on pCO_2 and pH are significantly smaller than that of AR, because DIC and TA production from SR is nearly equal. CD accounts for the majority of pCO_2 reduction and pH increment along the salinity gradient particularly at low salinity. All peak values of ΔpCO_2 and ΔpH are closely related to where and how much DIC and TA are changed as well as the distinct buffer capacity for different carbonate parameters (Cai et al., 2017, 2021; Egleston et al., 2010). If there are no SR and CD mainly originated from mangrove sediments, the CO_2 effluxes would increase by 103.6, 22.9, and 3.1 mmol m^{-2} d^{-1}, meanwhile pH would decrease by 0.66, 0.39, and 0.12 units at low (2–10) to medium (11–20) to high salinity (21–29) zones. These numbers are much larger than the observed CO_2 flux (2.0 mmol m^{-2} d^{-1}) and the anthropogenic CO_2-induced ocean acidification (∼0.1 units), emphasizing the important role of SR and CD in mangrove sediments.

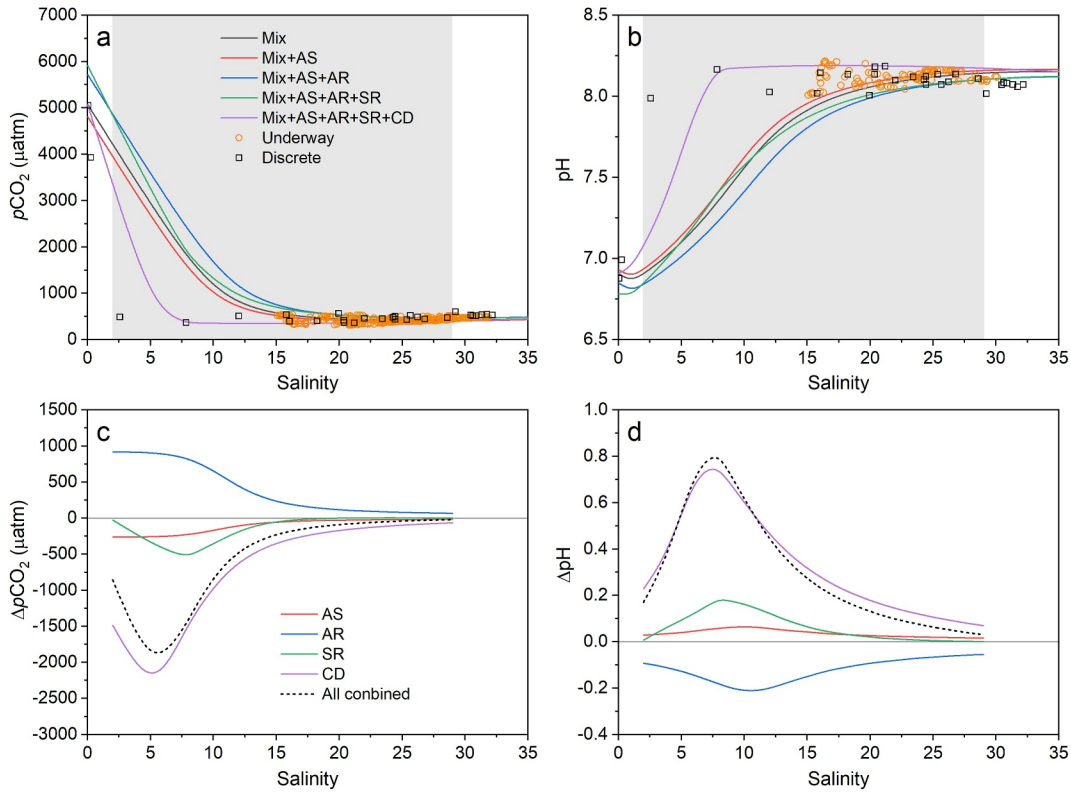

Figure 9. Model simulations of the evolution of pCO_2 (a), pH (b) and their changes (c, d) in Qinglan Harbor. The gray shaded areas indicate the solutions of mathematic equations for SR and CD are all positive and make sense. Note that the simulation was made under the cruise mean water temperature (30.80°C).

5. Conclusions

Tidal movement can significantly influence the spatial distributions of water properties in shallow tropical estuaries. In early summer, the Dongzhai Harbor and Qinglan Harbor behave as weak CO_2 sources with magnitudes of 4.0 and 2.0 mmol m^{-2} d^{-1}, respectively. However, the Xiaohai Lagoon became a CO_2 sink of −6.4 mmol m^{-2} d^{-1}. In mangrove estuaries, the combined effect of AR, SR, and CD is the major control on carbonate dynamics. Without SR and CD mainly from mangrove sediments, the CO_2 emission would be 23 times larger than the observed value, and the pH would decrease by 0.39 units on an estuary-wide scale. However, in a more confined tropical lagoon, strong primary production of benthic macroalgae followed by carbonate formation can also significantly alter aquatic DIC and TA. Either the lateral export of alkalinity from mangrove sediments or the in situ metabolism of macroalgae has a strong capacity to reduce the emission of Greenhouse Gas CO_2 and buffer the pH declines, which is of great importance to counter global climate change and ocean acidification. Our study emphasizes the priority to protect and restore the blue carbon ecosystem as vulnerable but valuable coastal carbon reserves.

Conflict of Interest

The authors declare no conflicts of interest relevant to this study.

Data Availability Statement

Research Data associated with this article can be accessed at Mendeley Data repository https://data.mendeley.com/datasets/z7shndysb4/1.

Acknowledgments
This research was funded by the Hainan Province Science and Technology Special Fund [Grants ZDYF2022SHFZ056, ZDYF2021SHFZ064], the National Natural Science Foundation of China [Grants 42306050, 42276043], the Innovation Fund for Scientific and Technological Personnel of Hainan Province [Grant KJRC2023B04], and the Research Start-up Funds of Hainan University [Grant KYQD(ZR)-22026]. This work was also supported by the MEL Visiting Fellowship [Grant MELRS2225]. We thank Youfei Fu and Siyi Zhao for their assistance in sampling and CTD profiling. We also thank Haikou Marine Center of the Ministry of Natural Resources for providing the wind speed data.

References

Akhand, A., Chanda, A., Watanabe, K., Das, S., Tokoro, T., Hazra, S., & Kuwae, T. (2021). Reduction in riverine freshwater supply changes inorganic and organic carbon dynamics and air-water CO_2 fluxes in a tropical mangrove dominated estuary. *Journal of Geophysical Research: Biogeosciences*, *126*(5), e2020JG006144. https://doi.org/10.1029/2020JG006144

Alling, V., Porcelli, D., Mörth, C. M., Anderson, L. G., Sanchez-Garcia, L., Gustafsson, Ö., et al. (2012). Degradation of terrestrial organic carbon, primary production and out-gassing of CO_2 in the Laptev and East Siberian Seas as inferred from $\delta^{13}C$ values of DIC. *Geochimica et Cosmochimica Acta*, *95*, 143–159. https://doi.org/10.1016/j.gca.2012.07.028

Alongi, D. M. (2014). Carbon cycling and storage in mangrove forests. *Annual Review of Marine Science*, *6*(1), 195–219. https://doi.org/10.1146/annurev-marine-010213-135020

Alongi, D. M. (2020). Carbon balance in salt marsh and mangrove ecosystems: A global synthesis. *Journal of Marine Science and Engineering*, *8*(10), 767. https://doi.org/10.3390/jmse8100767

Bao, H., Wu, Y., Tian, L., Zhang, J., & Zhang, G. (2013). Sources and distributions of terrigenous organic matter in a mangrove fringed small tropical estuary in South China. *Acta Oceanologica Sinica*, *32*(4), 18–26. https://doi.org/10.1007/s13131-013-0295-3

Borges, A. V. (2005). Do we have enough pieces of the jigsaw to integrate CO_2 fluxes in the coastal ocean? *Estuaries*, *28*(1), 3–27. https://doi.org/10.1007/BF02732750

Borges, A. V., Djenidi, S., Lacroix, G., Théate, J., Delille, B., & Frankignoulle, M. (2003). Atmospheric CO_2 flux from mangrove surrounding waters. *Geophysical Research Letters*, *30*(11), 1558. https://doi.org/10.1029/2003GL017143

Borges, A. V., Vanderborght, J.-P., Schiettecatte, L.-S., Gazeau, F., Ferrón-Smith, S., Delille, B., & Frankignoulle, M. (2004). Variability of the gas transfer velocity of CO_2 in a macrotidal estuary (the Scheldt). *Estuaries*, *27*(4), 593–603. https://doi.org/10.1007/BF02907647

Bouillon, S., Dehairs, F., Velimirov, B., Abril, G., & Borges, A. V. (2007). Dynamics of organic and inorganic carbon across contiguous mangrove and seagrass systems (Gazi Bay, Kenya). *Journal of Geophysical Research*, *112*(G2), G02018. https://doi.org/10.1029/2006JG000325

Cabral, A., Dittmar, T., Call, M., Scholten, J., de Rezende, C. E., Asp, N., et al. (2021). Carbon and alkalinity outwelling across the groundwater-creek-shelf continuum off Amazonian mangroves. *Limnology and Oceanography Letters*, *6*(6), 369–378. https://doi.org/10.1002/lol2.10210

Cai, W.-J., Feely, R. A., Testa, J. M., Li, M., Evans, W., Alin, S. R., et al. (2021). Natural and anthropogenic drivers of acidification in large estuaries. *Annual Review of Marine Science*, *13*(1), 23–55. https://doi.org/10.1146/annurev-marine-010419-011004

Cai, W.-J. (2011). Estuarine and coastal ocean carbon paradox: CO_2 sinks or sites of terrestrial carbon incineration? *Annual Review of Marine Science*, *3*(1), 123–145. https://doi.org/10.1146/annurev-marine-120709-142723

Cai, W.-J., Dai, M., Wang, Y., Zhai, W., Huang, T., Chen, S., et al. (2004). The biogeochemistry of inorganic carbon and nutrients in the Pearl River estuary and the adjacent Northern South China Sea. *Continental Shelf Research*, *24*(12), 1301–1319. https://doi.org/10.1016/j.csr.2004.04.005

Cai, W.-J., Hu, X., Huang, W.-J., Murrell, M. C., Lehrter, J. C., Lohrenz, S. E., et al. (2011). Acidification of subsurface coastal waters enhanced by eutrophication. *Nature Geoscience*, *4*(11), 766–770. https://doi.org/10.1038/ngeo1297

Cai, W.-J., Huang, W.-J., Luther, G. W., Pierrot, D., Li, M., Testa, J., et al. (2017). Redox reactions and weak buffering capacity lead to acidification in the Chesapeake Bay. *Nature Communications*, *8*(1), 369. https://doi.org/10.1038/s41467-017-00417-7

Cai, W.-J., Luther, G. W., Cornwell, J. C., & Giblin, A. E. (2010). Carbon cycling and the coupling between proton and electron transfer reactions in aquatic sediments in Lake Champlain. *Aquatic Geochemistry*, *16*(3), 421–446. https://doi.org/10.1007/s10498-010-9097-9

Cai, W.-J., & Wang, Y. (1998). The chemistry, fluxes, and sources of carbon dioxide in the estuarine waters of the Satilla and Altamaha Rivers, Georgia. *Limnology & Oceanography*, *43*(4), 657–668. https://doi.org/10.4319/lo.1998.43.4.0657

Call, M., Maher, D. T., Santos, I. R., Ruiz-Halpern, S., Mangion, P., Sanders, C. J., et al. (2015). Spatial and temporal variability of carbon dioxide and methane fluxes over semi-diurnal and spring–neap–spring timescales in a mangrove creek. *Geochimica et Cosmochimica Acta*, *150*, 211–225. https://doi.org/10.1016/j.gca.2014.11.023

Call, M., Santos, I. R., Dittmar, T., de Rezende, C. E., Asp, N. E., & Maher, D. T. (2019). High pore-water derived CO_2 and CH_4 emissions from a macro-tidal mangrove creek in the Amazon region. *Geochimica et Cosmochimica Acta*, *247*, 106–120. https://doi.org/10.1016/j.gca.2018.12.029

Cao, Z., Dai, M., Zheng, N., Wang, D., Li, Q., Zhai, W., et al. (2011). Dynamics of the carbonate system in a large continental shelf system under the influence of both a river plume and coastal upwelling. *Journal of Geophysical Research*, *116*(G2), G02010. https://doi.org/10.1029/2010JG001596

Chen, B., Cai, W.-J., Brodeur, J. R., Hussain, N., Testa, J. M., Ni, W., & Li, Q. (2020). Seasonal and spatial variability in surface pCO_2 and air–water CO_2 flux in the Chesapeake Bay. *Limnology & Oceanography*, *65*(12), 3046–3065. https://doi.org/10.1002/lno.11573

Chen, C. T. A., Huang, T. H., Chen, Y. C., Bai, Y., He, X., & Kang, Y. (2013). Air-sea exchanges of CO_2 in the world's coastal seas. *Biogeosciences*, *10*(10), 6509–6544. https://doi.org/10.5194/bg-10-6509-2013

Chen, X., Call, M., Reithmaier, G., Maher, D., Holloway, C., Wadnerkar, P., et al. (2021). The mangrove CO_2 pump: Tidally driven pore-water exchange. *Limnology & Oceanography*, *66*(4), 1563–1577. https://doi.org/10.1002/lno.11704

Chen, X., Zhang, F., Lao, Y., Wang, X., Du, J., & Santos, I. R. (2018). Submarine groundwater discharge-derived carbon fluxes in mangroves: An important component of blue carbon budgets? *Journal of Geophysical Research: Oceans*, *123*(9), 6962–6979. https://doi.org/10.1029/2018JC014448

Chou, W.-C., Fan, L.-F., Yang, C.-C., Chen, Y.-H., Hung, C.-C., Huang, W.-J., et al. (2021). A unique diel pattern in carbonate chemistry in the seagrass meadows of Dongsha Island: The enhancement of metabolic carbonate dissolution in a semienclosed lagoon. *Frontiers in Marine Science*, *8*, 717685. https://doi.org/10.3389/fmars.2021.717685

Cotovicz, L. C., Knoppers, B. A., Régis, C. R., Tremmel, D., Costa-Santos, S., & Abril, G. (2021). Eutrophication overcoming carbonate precipitation in a tropical hypersaline coastal lagoon acting as a CO_2 sink (Araruama Lagoon, SE Brazil). *Biogeochemistry*, *156*(2), 231–254. https://doi.org/10.1007/s10533-021-00842-3

Cotovicz, L. C., Vidal, L. O., de Rezende, C. E., Bernardes, M. C., Knoppers, B. A., Sobrinho, R. L., et al. (2020). Carbon dioxide sources and sinks in the delta of the Paraíba do Sul River (Southeastern Brazil) modulated by carbonate thermodynamics, gas exchange and ecosystem metabolism during estuarine mixing. *Marine Chemistry*, *226*, 103869. https://doi.org/10.1016/j.marchem.2020.103869

Cotovicz, L. C., Ribeiro, R., Ramos Regis, C., Bernardes, M., Sobrinho, R., Vidal, L., et al. (2021). Greenhouse gas emissions (CO_2 and CH_4) and inorganic carbon behavior in an urban highly polluted tropical coastal lagoon (SE, Brazil). *Environmental Science and Pollution Research*, *28*, 38173–38192. https://doi.org/10.1007/s11356-021-13362-2

Egleston, E. S., Sabine, C. L., & Morel, F. M. M. (2010). Revelle revisited: Buffer factors that quantify the response of ocean chemistry to changes in DIC and alkalinity. *Global Biogeochemical Cycles*, *24*(1), GB1002. https://doi.org/10.1029/2008GB003407

Enríquez, S., & Schubert, N. (2014). Direct contribution of the seagrass Thalassia testudinum to lime mud production. *Nature Communications*, *5*(1), 3835. https://doi.org/10.1038/ncomms4835

Faber, P. A., Evrard, V., Woodland, R. J., Cartwright, I. C., & Cook, P. L. M. (2014). Pore-water exchange driven by tidal pumping causes alkalinity export in two intertidal inlets. *Limnology & Oceanography*, *59*(5), 1749–1763. https://doi.org/10.4319/lo.2014.59.5.1749

Fakhraee, M., Planavsky, N. J., & Reinhard, C. T. (2023). Ocean alkalinity enhancement through restoration of blue carbon ecosystems. *Nature Sustainability*, *6*(9), 1087–1094. https://doi.org/10.1038/s41893-023-01128-2

Fluet-Chouinard, E., Stocker, B. D., Zhang, Z., Malhotra, A., Melton, J. R., Poulter, B., et al. (2023). Extensive global wetland loss over the past three centuries. *Nature*, *614*(7947), 281–286. https://doi.org/10.1038/s41586-022-05572-6

Guo, X., & Wong, G. T. F. (2015). Carbonate chemistry in the Northern South China Sea Shelf-sea in June 2010. *Deep-Sea Research II*, *117*, 119–130. https://doi.org/10.1016/j.dsr2.2015.02.024

Guo, X., Dai, M., Zhai, W., Cai, W.-J., & Chen, B. (2009). CO_2 flux and seasonal variability in a large subtropical estuarine system, the Pearl River Estuary, China. *Journal of Geophysical Research*, *114*(G3). https://doi.org/10.1029/2008JG000905

Ho, D. T., Coffineau, N., Hickman, B., Chow, N., Koffman, T., & Schlosser, P. (2016). Influence of current velocity and wind speed on air-water gas exchange in a mangrove estuary. *Geophysical Research Letters*, *43*(8), 3813–3821. https://doi.org/10.1002/2016GL068727

Ho, D. T., Ferrón, S., Engel, V. C., Larsen, L. G., & Barr, J. G. (2014). Air-water gas exchange and CO_2 flux in a mangrove-dominated estuary. *Geophysical Research Letters*, *41*(1), 108–113. https://doi.org/10.1002/2013GL058785

Hu, X., & Cai, W.-J. (2013). Estuarine acidification and minimum buffer zone—A conceptual study. *Geophysical Research Letters*, *40*(19), 5176–5181. https://doi.org/10.1002/grl.51000

Huang, W. J., Wang, Y., & Cai, W. J. (2012). Assessment of sample storage techniques for total alkalinity and dissolved inorganic carbon in seawater. *Limnology and Oceanography: Methods*, *10*(9), 711–717. https://doi.org/10.4319/lom.2012.10.711

Jiang, L.-Q., Cai, W.-J., & Wang, Y. (2008). A comparative study of carbon dioxide degassing in river- and marine-dominated estuaries. *Limnology & Oceanography*, *53*(6), 2603–2615. https://doi.org/10.4319/lo.2008.53.6.2603

Joesoef, A., Huang, W. J., Gao, Y., & Cai, W. J. (2015). Air–water fluxes and sources of carbon dioxide in the Delaware Estuary: Spatial and seasonal variability. *Biogeosciences*, *12*(20), 6085–6101. https://doi.org/10.5194/bg-12-6085-2015

Kanamori, S., & Ikegami, H. (1980). Computer-processed potentiometric titration for the determination of calcium and magnesium in sea water. *Journal of the Oceanographical Society of Japan*, *36*(4), 177–184. https://doi.org/10.1007/bf02070330

Koné, Y. J. M., Abril, G., Kouadio, K. N., Delille, B., & Borges, A. V. (2009). Seasonal variability of carbon dioxide in the rivers and lagoons of Ivory Coast (West Africa). *Estuaries and Coasts*, *32*(2), 246–260. https://doi.org/10.1007/s12237-008-9121-0

Kremer, J. N., Reischauer, A., & D'Avanzo, C. (2003). Estuary-specific variation in the air-water gas exchange coefficient for oxygen. *Estuaries*, *26*(4), 829–836. https://doi.org/10.1007/BF02803341

Kristensen, E., Andersen, F. O., Holmboe, N., Holmer, M., & Thongtham, N. (2000). Carbon and nitrogen mineralization in sediments of the Bangrong mangrove area, Phuket, Thailand. *Aquatic Microbial Ecology*, *22*, 199–213. https://doi.org/10.3354/ame022199

Laruelle, G. G., Dürr, H. H., Lauerwald, R., Hartmann, J., Slomp, C. P., Goossens, N., & Regnier, P. A. G. (2013). Global multi-scale segmentation of continental and coastal waters from the watersheds to the continental margins. *Hydrology and Earth System Sciences*, *17*(5), 2029–2051. https://doi.org/10.5194/hess-17-2029-2013

Li, C., Cai, R., & Yan, X. (2020). Analysis on the changes of carbon budget of mangrove wetland in Hainan Dongzhaigang during 2010-2018. *Marine Science Bulletin*, *39*(4), 488–497. https://doi.org/10.11840/j.issn.1001-6392.2020.04.012

Liang, X., Zhao, H., He, Y., Zhu, L., Zou, Y., & Ye, C. (2022). Spatiotemporal characteristics of agricultural nitrogen and phosphorus emissions to water and its source identification: A case in Bamen Bay, China. *Journal of Contaminant Hydrology*, *245*, 103936. https://doi.org/10.1016/j.jconhyd.2021.103936

Liu, B., Xia, P., Du, J., Luo, X., Zhai, R., & Lin, J. (2024). Sedimentary records of environmental evolution in Dongzhai Port mangrove swamps (South China) over the last hundred years: Insights from corrections of grain-size effects. *Environmental Pollution*, *343*, 123179. https://doi.org/10.1016/j.envpol.2023.123179

Liu, X., & Ge, C. (2012). Spatial and temporal variations of sedimented organic matter in Xiaohai Lagoon, Hainan Island. *Acta Oceanologica Sinica*, *31*(3), 74–86. https://doi.org/10.1007/s13131-012-0208-x

Maher, D. T., Cowley, K., Santos, I. R., Macklin, P., & Eyre, B. D. (2015). Methane and carbon dioxide dynamics in a subtropical estuary over a diel cycle: Insights from automated in situ radioactive and stable isotope measurements. *Marine Chemistry*, *168*, 69–79. https://doi.org/10.1016/j.marchem.2014.10.017

Maher, D. T., & Eyre, B. D. (2012). Carbon budgets for three autotrophic Australian estuaries: Implications for global estimates of the coastal air-water CO_2 flux. *Global Biogeochemical Cycles*, *26*(1), GB1032. https://doi.org/10.1029/2011GB004075

Maher, D. T., Santos, I. R., Golsby-Smith, L., Gleeson, J., & Eyre, B. D. (2013). Groundwater-derived dissolved inorganic and organic carbon exports from a mangrove tidal creek: The missing mangrove carbon sink? *Limnology & Oceanography*, *58*(2), 475–488. https://doi.org/10.4319/lo.2013.58.2.0475

Ray, R., Thouzeau, G., Walcker, R., Vantrepotte, V., Gleixner, G., Morvan, S., et al. (2020). Mangrove-derived organic and inorganic carbon exchanges between the Sinnamary Estuarine System (French Guiana, South America) and Atlantic Ocean. *Journal of Geophysical Research: Biogeosciences*, *125*(8), e2020JG005739. https://doi.org/10.1029/2020JG005739

Raymond, P. A., & Cole, J. J. (2001). Gas exchange in rivers and estuaries: Choosing a gas transfer velocity. *Estuaries*, *24*(2), 312–317. https://doi.org/10.2307/1352954

Reithmaier, G. M. S., Cabral, A., Akhand, A., Bogard, M. J., Borges, A. V., Bouillon, S., et al. (2023). Carbonate chemistry and carbon sequestration driven by inorganic carbon outwelling from mangroves and saltmarshes. *Nature Communications*, *14*(1), 8196. https://doi.org/10.1038/s41467-023-44037-w

Reithmaier, G. M. S., Ho, D. T., Johnston, S. G., & Maher, D. T. (2020). Mangroves as a source of greenhouse gases to the atmosphere and alkalinity and dissolved carbon to the coastal ocean: A case study from the Everglades National Park, Florida. *Journal of Geophysical Research: Biogeosciences*, *125*(12), e2020JG005812. https://doi.org/10.1029/2020JG005812

Reithmaier, G. M. S., Johnston, S. G., Junginger, T., Goddard, M. M., Sanders, C. J., Hutley, L. B., et al. (2021). Alkalinity production coupled to pyrite formation represents an unaccounted blue carbon sink. *Global Biogeochemical Cycles*, *35*(4), e2020GB006785. https://doi.org/10.1029/2020GB006785

Rosentreter, J. A., & Eyre, B. D. (2025). Uncertainties about the role of river and mangrove dissolved inorganic carbon and alkalinity loads in buffering the Great Barrier Reef Lagoon. *Global Biogeochemical Cycles*, *39*(1), e2024GB008134. https://doi.org/10.1029/2024GB008134

Rosentreter, J. A., Laruelle, G. G., Bange, H. W., Bianchi, T. S., Busecke, J. J. M., Cai, W.-J., et al. (2023). Coastal vegetation and estuaries are collectively a greenhouse gas sink. *Nature Climate Change*, *13*(6), 579–587. https://doi.org/10.1038/s41558-023-01682-9

Rosentreter, J. A., Maher, D. T., Erler, D. V., Murray, R., & Eyre, B. D. (2018). Seasonal and temporal CO_2 dynamics in three tropical mangrove creeks—A revision of global mangrove CO_2 emissions. *Geochimica et Cosmochimica Acta*, *222*, 729–745. https://doi.org/10.1016/j.gca.2017.11.026

Rosentreter, J. A., Maher, D. T., Ho, D. T., Call, M., Barr, J. G., & Eyre, B. D. (2017). Spatial and temporal variability of CO_2 and CH_4 gas transfer velocities and quantification of the CH_4 microbubble flux in mangrove dominated estuaries. *Limnology & Oceanography*, *62*(2), 561–578. https://doi.org/10.1002/lno.10444

Saderne, V., Fusi, M., Thomson, T., Dunne, A., Mahmud, F., Roth, F., et al. (2021). Total alkalinity production in a mangrove ecosystem reveals an overlooked Blue Carbon component. *Limnology and Oceanography Letters*, *6*(2), 61–67. https://doi.org/10.1002/lol2.10170

Samanta, S., Dalai, T. K., Pattanaik, J. K., Rai, S. K., & Mazumdar, A. (2015). Dissolved inorganic carbon (DIC) and its $\delta^{13}C$ in the Ganga (Hooghly) River estuary, India: Evidence of DIC generation via organic carbon degradation and carbonate dissolution. *Geochimica et Cosmochimica Acta*, *165*, 226–248. https://doi.org/10.1016/j.gca.2015.05.040

Santos, I. R., Burdige, D. J., Jennerjahn, T. C., Bouillon, S., Cabral, A., Serrano, O., et al. (2021). The renaissance of Odum's outwelling hypothesis in "Blue Carbon" science. *Estuarine, Coastal and Shelf Science*, *255*, 107361. https://doi.org/10.1016/j.ecss.2021.107361

Santos, I. R., Eyre, B. D., & Huettel, M. (2012). The driving forces of porewater and groundwater flow in permeable coastal sediments: A review. *Estuarine, Coastal and Shelf Science*, *98*, 1–15. https://doi.org/10.1016/j.ecss.2011.10.024

Santos, I. R., Maher, D. T., Larkin, R., Webb, J. R., & Sanders, C. J. (2019). Carbon outwelling and outgassing vs. burial in an estuarine tidal creek surrounded by mangrove and saltmarsh wetlands. *Limnology & Oceanography*, *64*(3), 996–1013. https://doi.org/10.1002/lno.11090

Sippo, J. Z., Maher, D. T., Tait, D. R., Holloway, C., & Santos, I. R. (2016). Are mangroves drivers or buffers of coastal acidification? Insights from alkalinity and dissolved inorganic carbon export estimates across a latitudinal transect. *Global Biogeochemical Cycles*, *30*(5), 753–766. https://doi.org/10.1002/2015GB005324

Su, J., Cai, W.-J., Brodeur, J., Chen, B., Hussain, N., Yao, Y., et al. (2020). Chesapeake Bay acidification buffered by spatially decoupled carbonate mineral cycling. *Nature Geoscience*, *13*(6), 441–447. https://doi.org/10.1038/s41561-020-0584-3

Su, J., Cai, W.-J., Brodeur, J., Hussain, N., Chen, B., Testa, J. M., et al. (2020). Source partitioning of oxygen-consuming organic matter in the hypoxic zone of the Chesapeake Bay. *Limnology & Oceanography*, *65*(8), 1801–1817. https://doi.org/10.1002/lno.11419

Su, J., Cai, W.-J., Hussain, N., Brodeur, J., Chen, B., & Huang, K. (2019). Simultaneous determination of dissolved inorganic carbon (DIC) concentration and stable isotope ($\delta^{13}C$-DIC) by Cavity Ring-Down Spectroscopy: Application to study carbonate dynamics in the Chesapeake Bay. *Marine Chemistry*, *215*, 103689. https://doi.org/10.1016/j.marchem.2019.103689

Su, J., Dai, M., He, B., Wang, L., Gan, J., Guo, X., et al. (2017). Tracing the origin of the oxygen-consuming organic matter in the hypoxic zone in a large eutrophic estuary: The lower reach of the Pearl River Estuary, China. *Biogeosciences*, *14*(18), 4085–4099. https://doi.org/10.5194/bg-14-4085-2017

Su, N., Du, J., Moore, W. S., Liu, S., & Zhang, J. (2011). An examination of groundwater discharge and the associated nutrient fluxes into the estuaries of eastern Hainan Island, China using ^{226}Ra. *Science of the Total Environment*, *409*(19), 3909–3918. https://doi.org/10.1016/j.scitotenv.2011.06.017

Taillardat, P., Ziegler, A., Friess, D., Widory, D., Van Vinh, T., David, F., et al. (2018). Carbon dynamics and inconstant porewater input in a mangrove tidal creek over contrasting seasons and tidal amplitudes. *Geochimica et Cosmochimica Acta*, *237*, 32–48. https://doi.org/10.1016/j.gca.2018.06.012

Tait, D. R., Maher, D. T., Macklin, P. A., & Santos, I. R. (2016). Mangrove pore water exchange across a latitudinal gradient. *Geophysical Research Letters*, *43*(7), 3334–3341. https://doi.org/10.1002/2016GL068289

Taylor, J. R. (1997). Chapter 3. Propagation of uncertainties. In A. McGuire (Ed.), *An introduction to error analysis* (pp. 45–79). University Science Books. Sausalito.

Thibault de Chanvalon, A., Luther, G. W., Estes, E. R., Necker, J., Tebo, B. M., Su, J., & Cai, W. J. (2023). Influence of manganese cycling on alkalinity in the redox stratified water column of Chesapeake Bay. *Biogeosciences*, *20*(14), 3053–3071. https://doi.org/10.5194/bg-20-3053-2023

Volta, C., Ho, D. T., Maher, D. T., Wanninkhof, R., Friederich, G., Del Castillo, C., & Dulai, H. (2020). Seasonal variations in dissolved carbon inventory and fluxes in a mangrove-dominated estuary. *Global Biogeochemical Cycles*, *34*(12), e2019GB006515. https://doi.org/10.1029/2019GB006515

Wanninkhof, R. (1992). Relationship between wind speed and gas exchange over the ocean. *Journal of Geophysical Research*, *97*(C5), 7373–7382. https://doi.org/10.1029/92jc00188

Wanninkhof, R. (2014). Relationship between wind speed and gas exchange over the ocean revisited. *Limnology and Oceanography: Methods*, *12*(6), 351–362. https://doi.org/10.4319/lom.2014.12.351

Weiss, R. F. (1974). Carbon dioxide in water and seawater: The solubility of a non-ideal gas. *Marine Chemistry*, *2*(3), 203–215. https://doi.org/10.1016/0304-4203(74)90015-2

Wu, Z., Zhu, H., Tang, D., Wang, Y., Zidan, A., & Cui, Z. (2021). Submarine groundwater discharge as a significant export of dissolved inorganic carbon from a mangrove tidal creek to Qinglan Bay (Hainan Island, China). *Continental Shelf Research*, *223*, 104451. https://doi.org/10.1016/j.csr.2021.104451

Xu, Y.-Y., Pierrot, D., & Cai, W.-J. (2017). Ocean carbonate system computation for anoxic waters using an updated CO2SYS program. *Marine Chemistry*, *195*, 90–93. https://doi.org/10.1016/j.marchem.2017.07.002

Xue, L., & Cai, W.-J. (2020). Total alkalinity minus dissolved inorganic carbon as a proxy for deciphering ocean acidification mechanisms. *Marine Chemistry*, *222*, 103791. https://doi.org/10.1016/j.marchem.2020.103791

Yin, H., Jin, L., & Hu, X. (2024). Interpreting biogeochemical processes through the relationship between total alkalinity and dissolved inorganic carbon: Theoretical basis and limitations. *Limnology and Oceanography: Methods*, *22*(5), 311–320. https://doi.org/10.1002/lom3.10608

References From the Supporting Information

Geng, X., Cai, Z., Jia, S., Shen, J., Tang, D., Wang, D., & Chen, S. (2022). Environmental determinants of the distribution of Halophila beccarii Ascherson in Hainan Island, China. *Sustainability*, *14*(20), 13491. https://doi.org/10.3390/su142013491

Guo, X., Cai, W.-J., Zhai, W., Dai, M., Wang, Y., & Chen, B. (2008). Seasonal variations in the inorganic carbon system in the Pearl River (Zhujiang) estuary. *Continental Shelf Research*, *28*(12), 1424–1434. https://doi.org/10.1016/j.csr.2007.07.011

Herbeck, L. S., Unger, D., Krumme, U., Liu, S. M., & Jennerjahn, T. C. (2011). Typhoon-induced precipitation impact on nutrient and suspended matter dynamics of a tropical estuary affected by human activities in Hainan, China. *Estuarine, Coastal and Shelf Science*, *93*(4), 375–388. https://doi.org/10.1016/j.ecss.2011.05.004

Hu, J., Xin, K., Li, Z., Gao, C., & Yan, K. (2015). Carbon storage and sequestration function evaluation in Dongzhaigang Mangrove Reserve of Hainan. *Wetland Science*, *13*(3), 338–343. https://doi.org/10.13248/j.cnki.wetlandsci.2015.03.011

Nong, S.-Q., Yang, X.-B., Li, D.-H., Yang, L.-R., Xu, Z.-L., Chen, Y.-K., & Luo, Z.-M. (2011). Vegetation composition in the Mangrove Forest Nature protection area of Qinglan, China. *Plant Science Journal*, *1*(4), 459–466. https://doi.org/10.3724/SP.J.1142.2011.40459

Unger, D., Herbeck, L. S., Li, M., Bao, H., Wu, Y., Zhang, J., & Jennerjahn, T. (2013). Sources, transformation and fate of particulate amino acids and hexosamines under varying hydrological regimes in the tropical Wenchang/Wenjiao Rivers and Estuary, Hainan, China. *Continental Shelf Research*, *57*, 44–58. https://doi.org/10.1016/j.csr.2012.02.014

Xue, B., Wang, Z., Wu, P., Lu, Y., & Diao, M. (2023). Effects of geomorphic-induced turbulence on horizontal mixing in the coastal lagoon Xiaohai in China. *Regional Studies in Marine Science*, *64*, 103048. https://doi.org/10.1016/j.rsma.2023.103048